Cloud radiative forcing at the Atmospheric Radiation Measurement Program Climate Research Facility: 2. Vertical redistribution of radiant energy by clouds

Gerald G. Mace,[1] Sally Benson,[1] and Seiji Kato[2]

Received 28 February 2005; revised 24 August 2005; accepted 2 December 2005; published 7 June 2006.

[1] Documentation of the effects of clouds on the radiant energy balance of the surface and atmosphere represents a shortcoming in the set of observations that are needed to ascertain the validity of climate model simulations. While clouds are known to cool the climate system from top of atmosphere (TOA) radiation budget studies, the redistribution of energy between the surface and atmosphere and within the atmosphere by clouds has not been examined in detail with observations. Using data collected at the Atmospheric Radiation Measurement Program (ARM) Southern Great Plains (SGP) site, we use measurements of cloud occurrence and structure together with a scheme to characterize the cloud microphysical and radiative properties to estimate the uncertainty in our ability to calculate the radiative forcing and effect of clouds at the top of atmosphere, the surface and within the atmosphere. We find that overcast clouds during 2000 tended to have a small net influence on the atmosphere (6 W m^{-2} ± 3 W m^{-2} of heating) with net TOA and surface cooling (25 W m^{-2} ± 3 W m^{-2} and 32 ± 3 W m^{-2}, respectively). These statistics mask a significant redistribution of radiant energy within the atmosphere by clouds where low overcast clouds resulted in strong atmospheric cooling (37 W m^{-2} ± 9 W m^{-2}), and thin high clouds resulted in warming (21 W m^{-2} ± 6 W m^{-2}) suggesting that accurate prediction of the phasing of these cloud types within meteorological features is important for capturing the essential feedbacks by clouds to the general circulation.

Citation: Mace, G. G., S. Benson, and S. Kato (2006), Cloud radiative forcing at the Atmospheric Radiation Measurement Program Climate Research Facility: 2. Vertical redistribution of radiant energy by clouds, *J. Geophys. Res.*, *111*, D11S91, doi:10.1029/2005JD005922.

1. Introduction

[2] Clouds tend to cool the climate system. This commonly accepted fact derives from analysis of top of atmosphere (TOA) radiation budget observations such as ERBE [*Barkstrom et al.*, 1990], ISCCP [*Rossow and Schiffer*, 1999] and now CERES [*Weilicki et al.*, 1998] that have been compiled using more than 2 decades of observations. This cooling arises from the difference between the longwave warming by clouds owing to blackbody emission temperatures colder than the clear-sky effective temperature and the shortwave cooling due to an increase of reflection of shortwave radiation by clouds. However, this cloud-induced TOA cooling is not evenly distributed spatially or temporally within the climate system. Because cloud liquid and ice do not strongly absorb solar radiation while these species absorb strongly in the thermal infrared, the cooling influence of clouds is largely experienced at the earth's surface while the radiative forcing of the atmosphere varies widely from strong cooling at the tops of optically thick clouds, to net heating in optically thin layers [*Webster and Stephens*, 1984; *Stephens*, 2005; *Rossow and Zhang*, 1995, hereinafter referred to as RZ95]. The atmospheric cloud-induced heating is a strong function of regional synoptic-scale variability [*Lau and Crane*, 1995; *Weaver and Ramanathan*, 1997]. It is this interplay between the vertically distributed radiative and latent heating with the large-scale dynamics of the atmosphere that drives the global hydrological cycle [*Webster*, 1994], and it is the distribution of diabatic heating within the atmosphere as a function of space and time that composes the feedback by clouds to the atmospheric circulation [*Stephens*, 2005]. Cloud heating in turn has a first-order influence on the general circulation of the atmosphere through creation and destruction of zonal and eddy available potential energy [*Stuhlmann and Smith*, 1988; *Webster and Stephens*, 1984]. It is largely this coupling between heating and circulation that will ultimately define the response of regional climates to global increases in radiatively active trace gasses, and it is these key diabatic feedbacks induced by clouds that are challenging for models of the earth's climate (GCMs) to predict with any confidence [*Tseloudis et al.*, 2000; *Norris and Weaver*, 2001].

[1]Department of Meteorology, University of Utah, Salt Lake City, Utah, USA.
[2]Center for Atmospheric Sciences, Hampton University, Hampton, Virginia, USA.

0148-0227/06/2005JD005922

[3] The satellite-based radiation budget data sets referenced above, when combined with radiative transfer models and other observations, have provided us with a rough conceptual understanding of the distribution of cloud-induced heating within the atmosphere and at the surface [e.g., RZ95, *Bergman and Hendon*, 1998; *Sohn*, 1999]. We know from the studies of RZ95 and *Chen et al.* [2000] that cloud feedbacks within the atmosphere reinforce the equator to pole temperature gradients owing to stronger net cooling by relatively warmer topped polar clouds compared to the net warming of cold-topped tropical clouds while the cloud heating feedbacks in the middle latitude storm tracks oppose the seasonal cycle with a net warming in the winter and cooling in the summer [*Weaver and Ramanathan*, 1997]. The longwave effects of tropical clouds that ultimately enhance the atmospheric motions on large scales are also balanced by strong shortwave cooling. This cooling has been shown by *Ramanathan and Collins* [1991] to act in concert with the large-scale dynamics [*Lau et al.*, 1996], to maintain sea surface temperatures within the equatorial region of the Pacific. In the same sense, the vast regions of stratocumulus in the eastern subtropical ocean basins, while having little direct effect on the diabatic heating of the atmosphere, exert a strong cooling influence on the subtropical oceans. In the absence of these boundary layer clouds, this region would absorb much of the solar energy the stratocumulus reflect to space. The ocean surface cooling is enhanced by evaporation brought about by the low-level easterlies of the Walker circulation driven by basin-scale radiative heating gradients [*Sohn*, 1999; *Webster and Stephens*, 1984; *Sherwood et al.*, 1994]. The net influence on ocean circulations and heat storage in the climate system is substantial [*Bergman and Hendon*, 2000]. Middle latitude clouds systems, on the other hand, tend to be associated with baroclinic eddies whose intensity and frequency are driven by the meridional temperature gradient. *Rossow and Zhang* [1995] suggest that middle latitude cloud systems exert little net radiative heating on the atmosphere. However, the vertical variability of the cloud induced heating is likely substantial [*Webster and Stephens*, 1984] although this variability has not been documented with data.

[4] This brief account of cloud feedbacks (see *Stephens* [2005] for an extensive review of the topic) suggests a complicated interplay between clouds and the climate system where the effects of clouds ranges from direct heating and cooling of the surface and atmosphere, to remote responses that are indirect but no less critical to the evolution of the atmospheric and oceanic general circulation. It is therefore no surprise that climate models find it a significant challenge to even approximate the feedback processes that are found in nature [*Stephens*, 2005]. This difficulty arises essentially because the properties of most cloud types in nature are determined by dynamical and physical processes that act well below the grid resolution of most GCMs and must be parameterized. These parameterizations are often not fully constrained by data and various components of a parameterization are therefore often considered to be free parameters that can be adjusted to force a model to match some set of observations. Traditionally, the ERBE observations from the middle and late 1980s have been used as an observational constraint on climate models and most established GCMs are able to match the TOA ERBE cloud effect to a reasonable approximation [*Kiehl et al.*, 1994]. While matching the TOA radiation budget is necessary, *Webster and Stephens* [1984] warned 20 years ago that validation of a GCM with TOA radiation budget data is not sufficient because cloud feedbacks in the atmosphere arise from a subtle redistribution of energy within the atmosphere and at the surface. Agreement between models and data at TOA can come about through compensating errors. In support of this assertion, *Stephens et al.* [2002] shows that even though models agree in quantities such as zonally averaged precipitation rate and TOA cloud radiative effects, their zonally averaged condensed water path can vary by as much as a factor of 3 or more. These problems have been highlighted by recent comparisons of model results with ISCCP cloud retrievals [e.g., *Zhang et al.*, 2005] and by segregating model results in terms of dynamical composites in order to isolate specific cloud feedback issues [*Tseloudis et al.*, 2000; *Norris and Weaver*, 2001]. It now seems clear that even though GCMs are able to match the TOA cloud effect of ERBE, this match is in fact obtained by nearly all models through compensating errors.

[5] While a global data set describing the vertical distribution of cloud properties is not yet available, a surrogate to such a data set has been created by the Atmospheric Radiation Measurement Program (ARM). In the work by *Mace et al.* [2006, hereinafter referred to as part 1], we present and evaluate a data analysis approach that uses the continuous measurements of the atmospheric thermodynamics and cloud structures measured at the Southern Great Plains (SGP) ARM site to characterize the microphysical and radiative properties of clouds and then use the results and a radiative transfer model to estimate the solar and thermal infrared flux profiles. The results compared favorably both in a case study evaluation and statistically with measurements of flux at the surface and TOA over a period of 1 year. Our goal in this paper is to examine the radiative effects of clouds and their association with the large-scale dynamics at the SGP ARM site during a particular month when an intensive observational program (IOP) was ongoing during March 2000 (section 3) as well as to examine the vertical redistribution of radiant energy by clouds during the entire year 2000 (section 5). In the next section, we review briefly the analysis technique and validation discussed in detail in part 1. We also consider, on the basis of the validation statistics in part 1, the quantitative uncertainty of the cloud radiative effect (i.e., W m^{-2} difference in the net flux due to clouds) and the radiative forcing (i.e., K day^{-1} heating rate) in the atmospheric profile.

2. Technique and Error Characterization

[6] As discussed in detail in part 1, our goal is to use the operational ARM data streams to characterize the physical state of the atmospheric profiles that are observed in the vertical column directly above the SGP instrument suite. In general, this description is created on a 5 min temporal and 90 m vertical grid, and uses many of the continuously operating active and passive remote sensors available at the ARM central facility. We begin with a description of the atmospheric thermodynamic profiles that are derived by merging the quasi regular radiosonde record created at the

SGP ARM site with other data. While the radiosonde record is extensive, the schedule has been irregular with time ranging from three hourly during intensive observing periods (IOPs) to no launches during nights and weekends during certain periods. Therefore we augment the radiosonde record with nearby radiosondes from the Norman Oklahoma National Weather Service site and from model output. The water vapor profile is normalized by water vapor column retrievals from the microwave radiometer (MWR), and the water vapor in the upper troposphere is further adjusted using the radiosonde correction suggested by *Miloshevich et al.* [2001]. These data are interpolated to the temporal and vertical resolution of our working grid.

[7] The occurrence and vertical structure of clouds are recorded by several vertically pointing active remote sensors at the SGP site that include laser ceilometers, a micropulse and Raman lidar, and a millimeter radar (MMCR). In the present study, we use the ceilometers to denote cloud base in the middle and lower troposphere and combine this with data from the MMCR to characterize the vertical profile of cloud properties. During the period of this study the MMCR recorded the first three moments of the Doppler spectrum including the radar reflectivity factor (Z_e,) the Doppler velocity (V_d) and the Doppler spectrum width. A data reduction algorithm that identifies cloud layers and merges the operational modes is applied to the data creating profiles every 36 s and these profiles are averaged into the 5 min temporal resolution.

[8] Cloud properties are derived from the remote sensing data using a suite of cloud property retrieval algorithms and parameterizations. Many such algorithms have been presented in the literature in recent years to retrieve the microphysical properties of cirrus clouds and liquid phase boundary layer clouds. For this initial study, we use the algorithm of *Dong and Mace* [2003] to derive the liquid phase cloud properties and the algorithms described by *Mace et al.* [2002] and *Mace et al.* [1998] for cirrus clouds. When neither of the cirrus algorithms are available, we use the *Liu and Illingworth* [2000] scheme. The complicating issue, however, is the existence of mixed phase clouds between the freezing level and about 243 K. Two issues must be dealt with. First, when supercooled clouds exist above warmer clouds, it is necessary to estimate what fraction of the column water path observed by the MWR is due to the warm clouds so that the *Dong and Mace* [2003] algorithm can be applied to the liquid phase layer. Second, it is necessary to determine the microphysical properties of the ice and liquid components. To address these issues, we use a parameterization of the liquid cloud profile by *Kiehl et al.* [1998] to first estimate the fraction of the observed liquid column that is warmer than freezing. Once estimated, we are able to apply the standard retrieval algorithms [*Dong and Mace*, 2003] to the warm clouds. The ice phase of mixed phase clouds are determined using a new parameterization of IWC as a function of V_d and Z_e derived from theory and regressed against aircraft measurements over the SGP site as discussed in detail in part 1. The liquid phase properties of mixed phase clouds are then derived using the cold fraction of the MWR water column and the *Kiehl et al.* [1998] parameterization from which particle sizes are also determined for the liquid and ice mixed phase components. Radiative properties are then calculated from parameterizations for liquid [*Slingo*, 1989; *Kiehl et al.*, 1998] and ice [*Fu*, 1996; *Fu et al.*, 1998]. Solar and IR radiative flux profiles are then calculated using a delta two stream radiative transfer algorithm [*Toon et al.*, 1989] with k-distribution method and correlated-k assumption given by *Kato et al.* [1999, 2001] for solar and *Mlawer et al.* [1997] for IR.

[9] The primary restrictions placed on application of this technique are that it cannot be implemented when the MWR is wet from dew or precipitation or when the MMCR observations are primarily derived from precipitation. Therefore we have developed empirical algorithms to identify such occurrences in the MWR data and we examine the MMCR data for the existence of a radar bright band, high reflectivities and strong Doppler velocities. Results from these periods are discarded in the following analysis.

[10] Validation of this technique is discussed in detail in part 1. While the cloud property retrieval algorithms have been validated to various degrees in the papers describing them, we compare the total column optical depth from the year 2000 with optical depths derived from retrieval of optical depth from the multifilter rotating shadowband radiometers (MFRSR) described by *Min and Harrison* [1996]. In uniform overcast skies during the year 2000 where the optical depth varies over 3 orders of magnitude we find a nearly unbiased comparison that is highly correlated. We also compare the TOA upwelling and surface downwelling thermal infrared and solar fluxes in overcast skies at SGP during the year 2000. The TOA fluxes are derived from a narrowband to broadband conversion algorithm [*Minnis et al.*, 1993]. At the surface, we compare the broadband longwave fluxes measured at the ARM site while for the solar flux, since we are not including aerosol, we compare the fraction of the clear sky solar flux removed by clouds using the estimated clear sky flux produced by *Long and Ackerman* [2000]. The results (Table 5 of part 1) showed high correlation with bias less than 10% for all quantities. The deviation about the linear regression line ranged from approximately 2% for the longwave downwelling to approximately 16% for the downwelling solar.

[11] We are attempting to explore in this paper the radiative effects of clouds on the atmospheric column over the ARM SGP site using column properties derived from the ARM data streams. Following RZ95, the cloud radiative effect (CRE) is defined as the difference between the cloudy and clear net fluxes in W m^{-2} at the TOA and surface while the atmospheric CRE is the difference between the TOA and surface values. The cloud radiative forcing (CRF) is defined as the convergence of radiant flux in a volume due to clouds (i.e., the difference between the cloudy and clear sky convergence of net flux) and is given in units of K day^{-1}. When averaged solar CRF and CRE are considered, the full diurnal cycle is generally included in the average. Quantitative evaluation of the uncertainty of the derived CRE and the CRF must be considered given the magnitude of the uncertainties in the cloud microphysical properties that propagate into uncertainties in the radiative flux calculations. For this error analysis, we use the standard error propagation theory developed by *Bevington and Robinson* [1992].

[12] The CRE can be written $C_x = (F_x \downarrow - F_x \uparrow)_{cloudy} - (F_x \downarrow - F_x \uparrow)_{clear}$ where the subscript x can be replaced with

(*s*, *TOA*), (*IR*, *TOA*), (*s*, *SFC*), and (*IR*, *SFC*), for the solar and IR effect at the TOA and surface respectively. This would allow us to express the variance, $\sigma^2_{CRE,x} = (\sigma^2_{F_x\downarrow} + \sigma^2_{F_x\uparrow})_{cloudy} + (\sigma^2_{F_x\downarrow} + \sigma^2_{F_x\uparrow})_{clear}$. At the TOA, we need consider only the upward fluxes (neglecting any uncertainties in the downwelling TOA solar flux) and at the surface we calculate the error in terms of the variance in the net fluxes, $\sigma^2_{CRE,x} = (\sigma^2_{F_{net,y}})_{cloudy} + (\sigma^2_{F_{net,y}})_{clear}$ where y denotes either solar or IR flux. Since the atmospheric CRE is just the difference between the CRE at the surface and TOA, we can express the uncertainty in the atmospheric CRE as $\sigma^2_{CRE,Atm,y} = (\sigma^2_{CRE,TOA,y}) + (\sigma^2_{CRE,Sfc,y})$ where we have neglected the error covariance between the surface and TOA which would tend to decrease the uncertainty (see below). Following *Bevington and Robinson* [1992], the uncertainty in the mean value of the cloud radiative effect taken over some number of realizations, $\overline{CRE}_x$, can be written

$$\sigma \frac{2}{CRE,x} = \frac{\sigma^2_{CRE}}{N} \tag{1}$$

where N is the number of instances composing $\overline{CRE}_x$. Using the statistics of the comparisons in part 1, we can then estimate the uncertainty in $\overline{CRE}_x$.

[13] The cloud radiative forcing is the convergence of net radiant flux into a volume. In practice we ignore the horizontal terms of the flux convergence and consider only the vertical component of flux. We approximate the vertical derivative with a simple centered difference formula:

$$H_y = -\frac{1}{\rho c_p}\frac{\partial F_{net,y}}{\partial z} \cong -\frac{1}{\rho c_p}\frac{F_{net,y_{+1}} - F_{net,y_{-1}}}{z_{+1} - z_{-1}}$$

where ρ is the air density, c_p is the specific heat at constant pressure, and z is the height and the subscripts +1 and −1 indicate the vertical levels above and below a level of interest. We are also primarily interested in the effects of clouds and therefore difference H_y in cloudy skies with a calculation that has cloud removed with no other changes to the temperature or moisture profiles. Considering only the first- and second-order terms that would contribute to the uncertainty in H, we can write,

$$\sigma^2_{H_y} \cong \frac{1}{\Delta z^2 \rho c_p}\left[\left(\sigma^2_{F_{+1,y}\uparrow} + \sigma^2_{F_{+1,y}\downarrow} + \sigma^2_{F_{-1,y}\uparrow} + \sigma^2_{F_{-1,y}\downarrow}\right) + 2\begin{pmatrix}\sigma^2_{F_{-1,y}\uparrow F_{-1,y}\downarrow} + \sigma^2_{F_{-1,y}\uparrow F_{+1,y}\uparrow} + \\ \sigma^2_{F_{-1,y}\uparrow F_{+1,y}\downarrow} + \sigma^2_{F_{-1,y}\downarrow F_{+1,y}\uparrow} + \sigma^2_{F_{-1,y}\downarrow F_{+1,y}\downarrow} + \sigma^2_{F_{+1,y}\downarrow F_{+1,y}\uparrow}\end{pmatrix}\right]$$

where $\Delta z^2 = (z_{+1} - z_{-1})^2$ and terms such as $\sigma^2_{F_{+1,y}\uparrow F_{+1,y}\downarrow}$ represent an error covariance of the indicated fluxes. The terms in the first parenthetical expression are a function of the uncertainties at the layer boundaries, and we approximate the downwelling error variance from the results of our analysis of the surface downwelling flux. Similarly, the upwelling flux variance is estimated using our TOA flux comparison results. In the second parenthetical expression, the terms that represent the covariance between the upwelling and downwelling fluxes are estimated by calculating the covariance between the flux errors at the surface and TOA while the terms that are covariances of upwelling or downwelling fluxes at different levels are assumed to be approximately represented by the variance of the upwelling or downwelling flux errors at the TOA and surface, respectively. With these approximations, we write

$$\sigma^2_{H_y} \cong \frac{1}{\Delta z^2 \rho c_p}\left[4\left(\sigma^2_{F_y\uparrow} + \sigma^2_{F_y\downarrow}\right) + 8\sigma^2_{F_y\uparrow F_y\downarrow}\right]. \tag{2}$$

In the analysis of the error covariance, we find a negative correlation between the downwelling surface radiation flux errors and the upwelling TOA flux errors ($r_{solar} = -0.69$, $r_{IR} = -0.23$). This negative correlation makes intuitive sense since an error resulting in too much (little) flux at the surface would imply (in the solar case) a cloud albedo that is too low (high) leading to too little (much) flux at the TOA compared to reality. Because the absorption is stronger in the IR and the values depend more on cloud base and top than on the optical depth, the correlation is less negative. The negative error covariance has the interesting implication of mitigating the heating error that would arise if the covariance were not included in equation (2).

[14] Assuming that equation (1) also applies to the CRF, Table 1 shows how the CRE and CRF uncertainties scale as a function of typical averaging times assuming 5 min data. Since we present the CRE and CRF in terms of means calculated over the entire diurnal cycle, we have simply halved our solar flux uncertainties and assumed the mean values of the downwelling flux for a given averaging period. There are several additional issues that should be considered regarding the uncertainty in the CRF and CRE. While the microphysical properties of many cloud types change rapidly in time, any errors in the microphysical retrievals in a given case may be correlated from one 5-min averaged column to the next. For the uncertainty analysis presented in Table 1 and in the results of the next section, we assume that these errors would decorrelate on timescales of approximately 30 min, and when calculating the CRE and CRF uncertainty, we simply divide the number of 5-min realizations by 6.

[15] The other issue that we have not addressed in this discussion or in Table 1 is the possibility of bias errors. Accounting for bias is critical since application of equation (1) to a long time series of data would tend to converge on the bias error. In part 1 we showed that the bias errors ranged from −5% for the surface net solar flux change due to clouds to +8% for our comparison to the TOA solar fluxes estimated from GOES data. For the IR downwelling at the surface and the solar downwelling at the surface (the observations that are likely the most accurately measured), the bias errors we obtain in overcast skies are less than 1%. However, this does not preclude higher biases at the TOA. In the IR, there is good reason to expect some bias due to the MMCR not sensing the optically tenuous tops of cloud layers while our simple treatment of the surface albedo where we take the measured broadband ratio of upwelling to downwelling solar flux and assume no spectral dependence may contribute to an upwelling solar bias. For our purpose here, we recognize that the errors calculated using the approach described in this section represents a minimum and that any biases will increase the reported errors.

Table 1. Approximate Uncertainty in the Indicated Quantities for Certain Approximate Averaging Times

	Hourly	Daily	Weekly	Monthly	Yearly
TOA solar CRE, W m^{-2}	41	12	4.5	2.2	1.1
TOA IR CRE, W m^{-2}	9	2.7	1.0	0.50	0.25
Atm solar CRE, W m^{-2}	42	16	4.6	2.3	1.2
Atm IR CRE, W m^{-2}	16	4.5	1.7	0.86	0.43
Sfc solar CRE, W m^{-2}	18	5.2	2.0	0.98	0.49
Sfc IR CRE, W m^{-2}	13	3.7	1.4	0.69	0.35
Solar heating rate, K day^{-1}	23	6.8	2.6	1.3	1.1
IR heating rate, K day^{-1}	15	4.2	1.6	0.80	0.40

[16] On the basis of their typical magnitudes, we find that we are able to reasonably estimate the TOA and surface CRE in both the solar and IR at most averaging times beyond a few hours. Since the atmospheric CRE is a residual of the TOA and surface values, longer averaging times are required to improve precision and for certain clouds, especially in the solar spectrum, the uncertainty will be substantial. Quantitative precision in the CRF is a greater concern. Near the tops and bottoms of cloud layers where the convergence of net flux is large, the cloud-induced heating can be several 10s of K day^{-1} instantaneously. Away from the bases and tops of layers, there is a residual cloud induced heating or cooling due to a change in the solar or infrared flux above and below the layer. This flux change modifies the gaseous absorption that would otherwise occur in clear skies. For instance an increase in the downwelling IR flux below a thick cloud layer will lead to a net cloud induced IR heating in that layer relative to the gaseous cooling that would typically occur. This secondary effect is small but persistent throughout the column and cannot be ignored in long-term averages. We find that our precision in solar heating is not generally sufficient to quantify CRF at cloud top or base in short averaging periods (order of several hours) although the sign of the IR forcing can often be reasonably estimated. Given the magnitudes of averaged heating and cooling in the atmosphere [*Webster and Stephens*, 1981], to obtain the precision needed to quantify CRF meaningfully requires very long averaging periods, and even then we find that our precision in the solar CRF remains marginal for quantitative purposes. Depending on the precision required for the question being addressed, cloud property retrieval algorithms of increased accuracy are needed to better characterize the column radiative properties and longer data records than 1 year are needed.

3. March 2000 Cloud IOP: Meteorology and Radiative Feedbacks

[17] Having a long-term description of the vertical column properties above the SGP central facility allows us to explore issues that are relevant to the cloud feedback problem. Here we examine in detail the evolution of the cloud properties and the cloud radiative forcings and their association with the large-scale dynamics during the month of March 2000 when several major intensive observational studies were ongoing at the ARM SGP. Given the diversity of conditions that were experienced during this month, March 2000 has emerged as focus of study by those interested in modeling the coupling of clouds with their dynamical environment. For instance, the ARM Cloud Parameterization and Modeling (CPM) group is focusing on this period as are the Global Energy and Water Cycle Experiment (GEWEX) Cloud System Study (GCSS) working group 3 as well as other GCSS working groups such as working group 2 who focus on high clouds. Given this interest and the importance of establishing a baseline against which models results can be compared, we describe the evolution of the cloud properties, their associated radiative heating and their association with the large-scale atmosphere.

[18] The 30 year March mean flow over the western 2/3 of the United States is shown in Figure 1 derived from NCEP/NCAR reanalysis data. During the typical March, we find a ridge located over the northwestern portion of the North American continent extending southward across the inter mountain west into the Great Basin. A mean trough exists near the California-Arizona border indicative of the frequent low-pressure systems that deepen and become cutoff from the midlatitude westerlies in this region. The subtropical jet is particularly active during the spring transition season. While there are similarities between the 30 year climatology and the March 2000 mean conditions (not shown), there are also significant differences represented by the anomalies in Figures 2a–2c where we separate the month into thirds that represent distinct dynamical regimes.

[19] During the first 9 days (Figure 2a), a high-amplitude geopotential height pattern existed over North America with a deep trough dominating the western half of the continent and a strong ridge over the east. During this period an active polar jet stream over the eastern Pacific provided a pathway for numerous midlatitude disturbances into western North America. The strong southwesterly flow in the upper troposphere across the middle third of the United States during the first 10 days of March allowed two major and several minor synoptic-scale weather systems to migrate from the desert southwest into the upper Mississippi valley. The first of the significant disturbances dominated the weather from 1 until 4 March. The evolution of the clouds and the meteorology for this period is discussed in detail in part 1. The second major system passed over the SGP region on 7 and 8 March when, unfortunately, the MMCR was inoperable during much of the period.

[20] The middle days of March 2000 were characterized by a much deamplified flow regime with numerous weak disturbances forming a mean trough that was situated over the central and southern plains (Figure 2b). These weak migratory disturbances were characterized by thick altostratus and cirrus on 12 and 13 March (Figure 3). By 15 March a slow moving thermal boundary in the low and middle

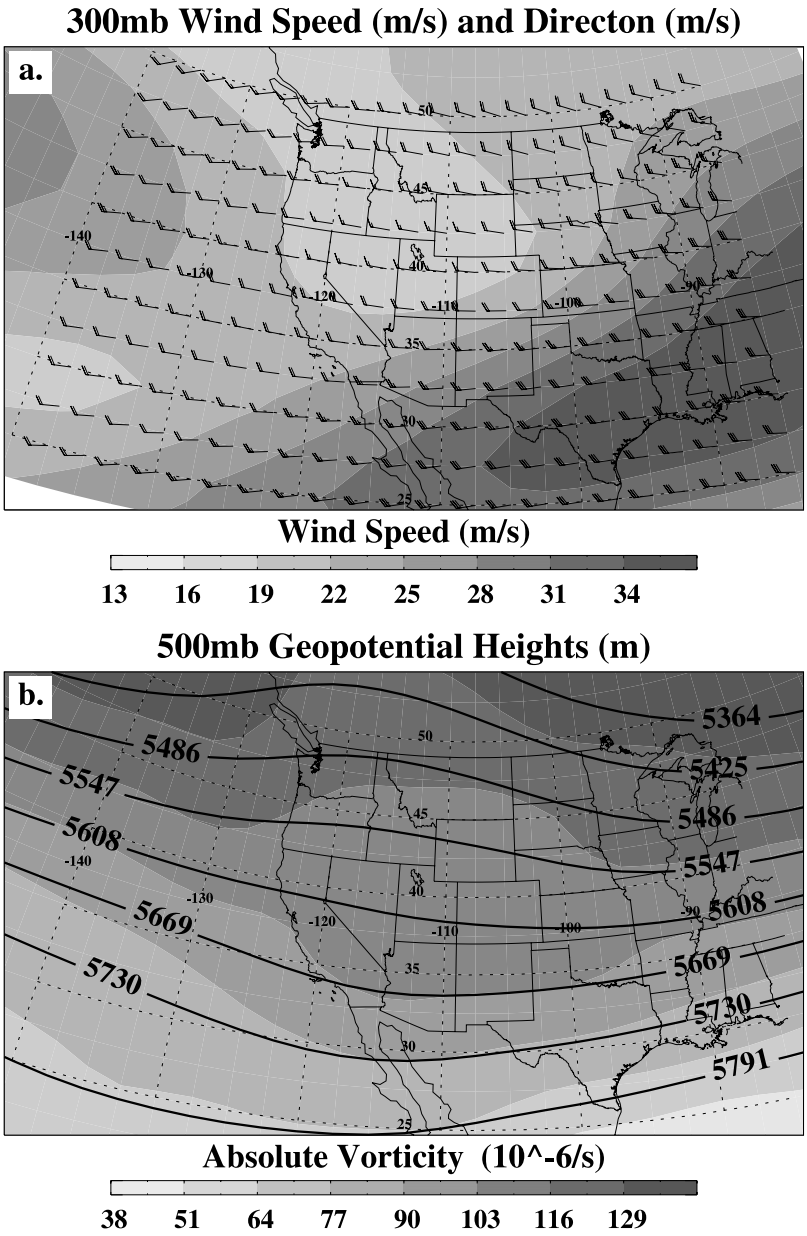

Figure 1. Thirty-year means of (a) 300 hPa wind velocity and (b) 500 hPa height and absolute vorticity for the month of March as derived from the NCEP/NCAR reanalysis data.

troposphere had settled over the central United States in nearly zonal flow in the middle and upper troposphere and a southerly flow in the lower levels brought northward a stream of moist air that overran the thermal boundary creating a prolonged period of cloud cover with occasional heavy rain between 15 and 19 March.

[21] Like the first third of the month, the latter third of March was characterized by a deep closed circulation at 500 mb over the southwestern United States. The strong Polar jet of the earlier period was displaced far northward by a strong eastern Pacific ridge while a somewhat stronger subtropical jet stream was active over the southwestern United States. A cutoff low was reforming over the desert southwest on 19 March as a vigorous migratory trough moved southeastward from the northern Rockies. This system formed a deep, nearly stationary low-pressure system over Arizona that caused extensive flooding in that area before the disturbance propagated northeastward passing the ARM SGP early on 24 March. Like the previous migratory cyclones that moved out of the desert southwest, the 24 March storm began with extensive cirrus 2 days before passage of the low-pressure center over the SGP. During the remainder of the month, migratory weather systems passed over the SGP region on a 3–4 day cycle resulting in fairly typical evolution of cloud patterns with cirrus followed by convection and rain that evolved into post frontal boundary layer clouds.

[22] As we see from the forgoing narrative, the meteorology during the month of March 2000 brought a rich diversity of conditions driven by a spectrum of migratory cyclones and weaker disturbances moving out of the desert southwest. In an effort to summarize the diabatic processes

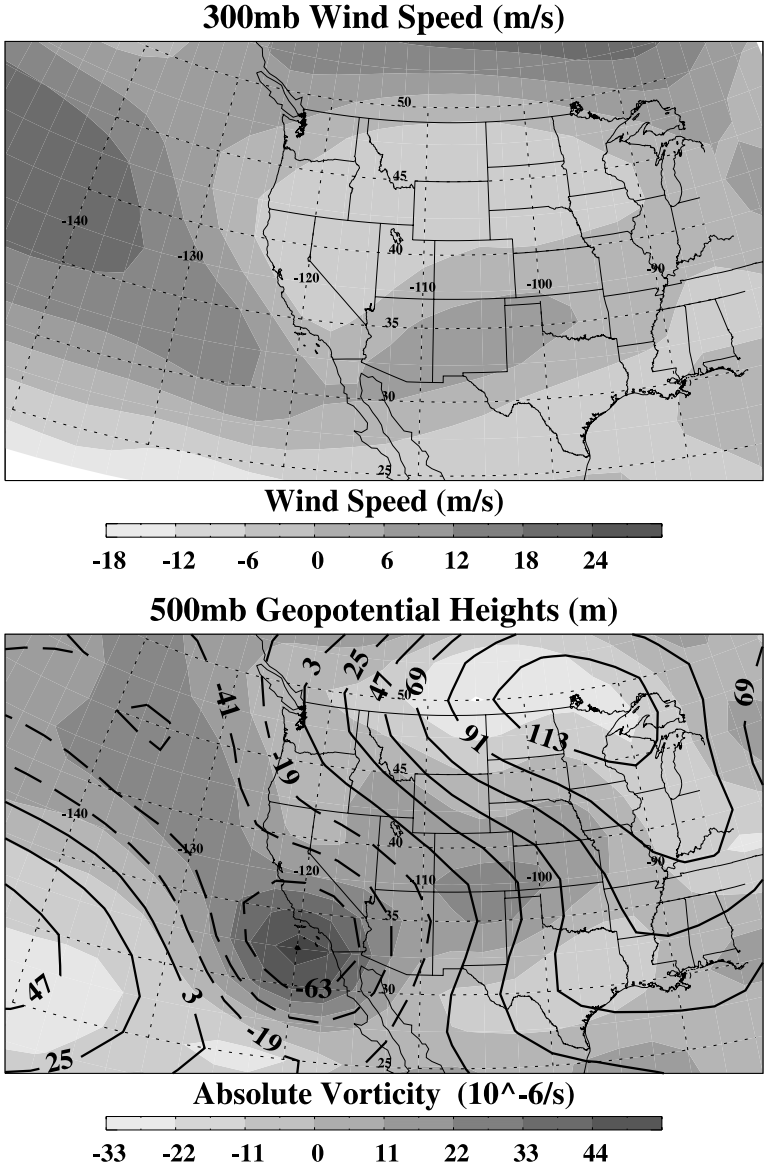

Figure 2a. Anomalies at 300 hPa and 500 hPa as labeled for the period 1–10 March 2000.

and their association with the large-scale atmosphere during March 2000, we show the calculated hourly averaged heating rates (keeping in mind the uncertainties), measured precipitation, and NCEP/NCAR large-scale vertical motion in Figure 4. Because Figure 4 is designed to show the general character of the relationships in a qualitative sense, we have not removed profiles that are possibly contaminated by precipitation, but we have denoted those periods with a symbol above the plot. We find a clear association between the diabatic heating and the large-scale vertical motion. Following the standard model put forth by *Lau and Crane* [1995, 1997], we find that the cirrus often occur ahead of the advancing weather systems in weak synoptic-scale vertical motions (1 March) or weak ascent (10 March) followed by deeper clouds associated with thermal boundaries and overrunning events. Stratocumulus often persists in the subsidence regions associated with cold air advection behind cold fronts (3, 19, and 30 March). The major weather events of March 2000 are clearly evident by periods of persistent synoptic-scale ascent and these periods are, without exception, associated with strong CRF and often precipitation (2, 10, 16, 23, and 29 March). The precipitation is generally episodic while the clouds are seen to exert a persistent radiative influence that is concentrated near cloud base and top. We find that the IR cloud top cooling is often quite diffuse and spread over several kilometers of depth when cloud tops occur in the upper troposphere (10, 13, 16, and 21 March) while this cooling is concentrated into a thinner layer when clouds are topped in the middle and lower troposphere (3, 17, 29, and 30 March). The IR heating near cloud bases tends to occur over a smaller vertical depth, while an IR heating rate of approximately 0.5 K day^{-1} is not uncommon below the bases of thick clouds. When cloud base is very low, the IR heating near cloud base is not substantial and the heating profile is determined by the general warming through the column until the cloud top

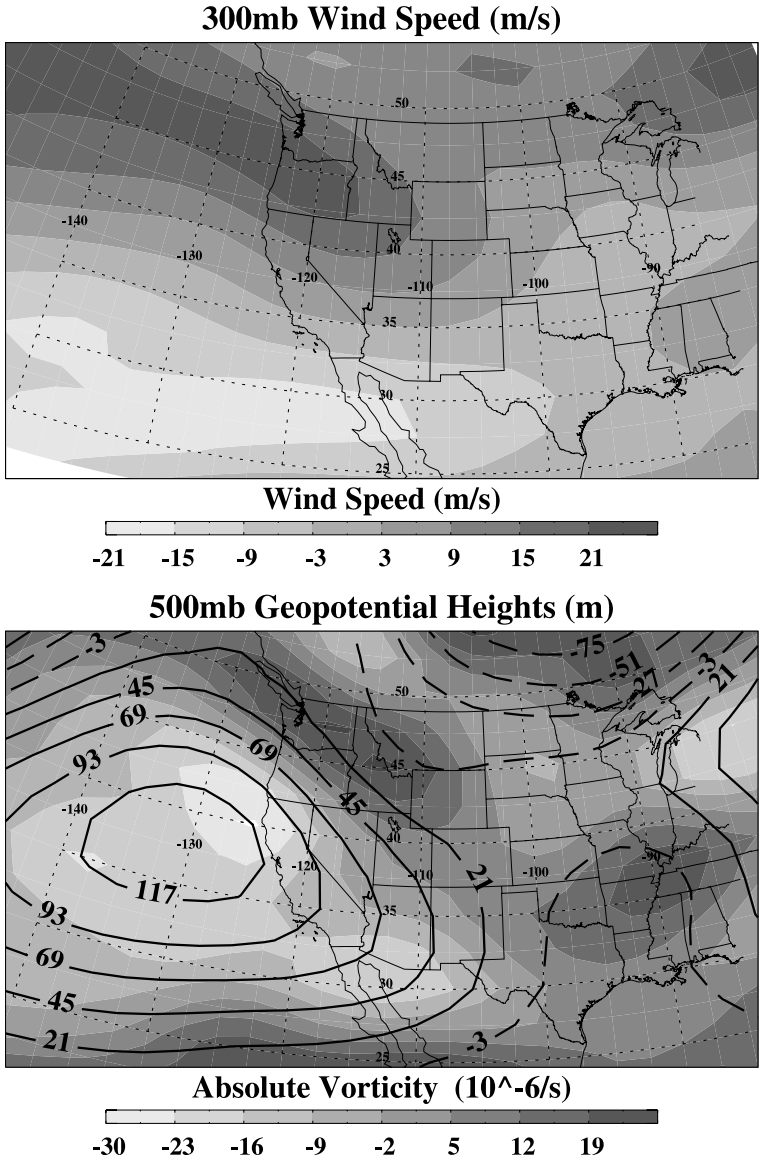

Figure 2b. As in Figure 2a except for 11–20 March 2000.

cooling becomes predominant (17–20 March). We find that the solar heating tends to mitigate the cloud top cooling when clouds occur during midday periods.

[23] The heating time height-time sections show that the redistribution of energy within the atmosphere is a complicated function of the vertical distribution of cloud optical thickness, cloud base and top heights, the time of day when the clouds occur, among other factors. It is a bit more straightforward to consider more quantitatively the CRE since this quantity essentially reduces the complex patterns of heating into how the clouds are energetically influencing the radiation streams at the surface, the TOA and within the atmosphere. Figures 5a–5c, shows the time series of the hourly averaged CRE during March 2000. The CRE is essentially the difference between the net cloudy and clear fluxes at the TOA and surface while the atmosphere CRE can be calculated as either the difference between the surface and TOA CRE or by summing the CRE at each level in a vertical column. The atmospheric CRE in Figure 5c was calculated both ways with agreement within 0.01 W m^{-2} generally.

[24] With the exception of clouds in the tops of ground-based inversions (which occurs in the polar regions routinely), clouds reduce the upwelling TOA longwave and increase the downwelling IR radiation at the surface over what would exist in clear skies. Therefore the IR CRE at the surface and TOA are always positive numbers with a magnitude at the surface that depends on the warmth of the lowest few optical depths of the layer and at the TOA that depends on the temperature of the upper few optical depths. It is fairly straightforward to move through the time series and follow the existence of clouds in the vertical column with the TOA and surface IR CRE. What is interesting is the effect of clouds on the atmosphere CRE. Optically thin clouds such as cirrus (1, 6, 9, and 28 March) are found to warm the atmosphere since they reduce the

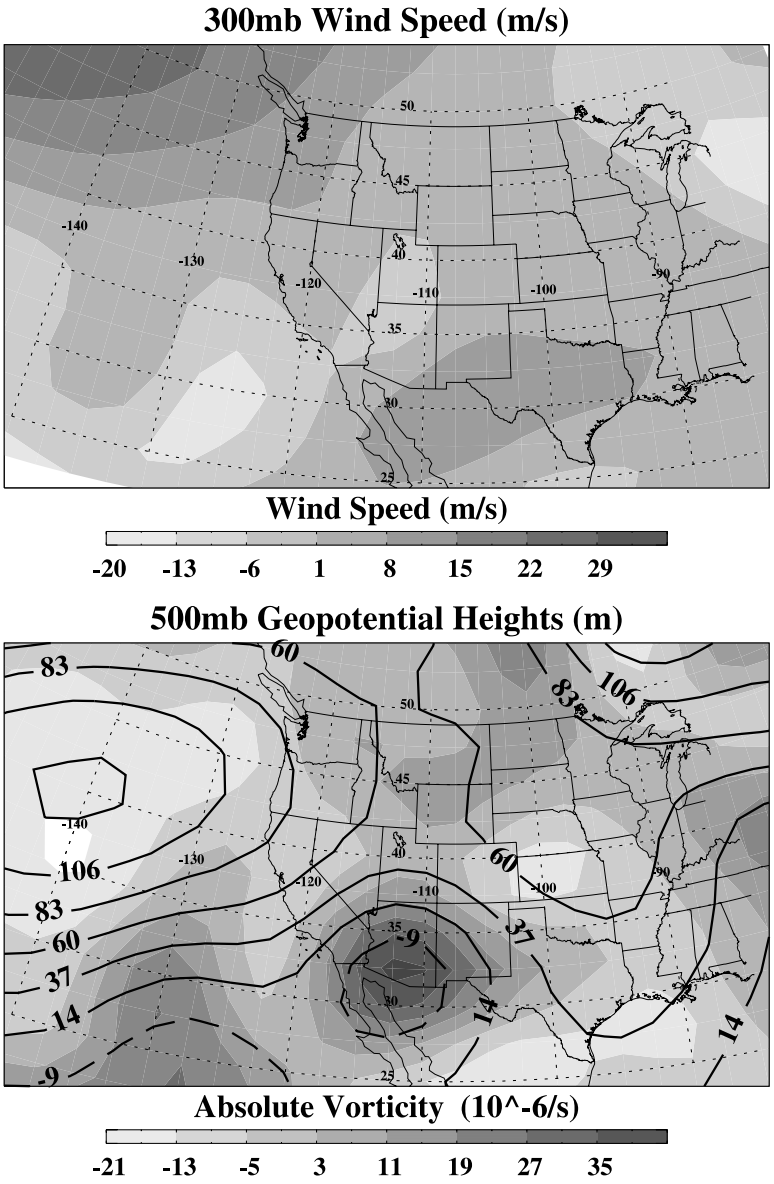

Figure 2c. As in Figure 2a except for 21–31 March 2000.

OLR more than they increase the downwelling surface longwave. Clouds that are optically thick result in a net cooling of the atmosphere that depends on the details of the vertical distribution of optical depth and the location of the layer, with this effect being enhanced for clouds that are vertically extended with high water loadings (2, 15, 18, and 19 March). Layers that seem to exist on the boundary between what we would normally consider cirrus and altostratus (12, 13, and 26 March) seem to alternate between IR heating and cooling depending on height and optical thickness. For instance, on 13 March, a layer descended during the afternoon and became progressively optically thicker reaching a maximum optical depth of approximately 25 between 2100 and 2200 UTC. The sign of the IR CRE switches during this period starting out with fairly strong warming as the layer was optically thick and cold. The layer eventually strongly cools the atmosphere as it becomes warmer but remained optically thick. Similar scenarios evolved on 12 and 21 March.

[25] The solar CRE, which is presented in absolute terms and as a fraction of the downwelling solar clear sky flux, shows that cloud-induced solar cooling of the vertical column is realized primarily at the surface where it is largely a function of the cloud optical depth. The atmosphere does tend to gain significant energy (compared to the IR) because of the absorption of solar energy by condensate although we find some regions where the atmospheric solar CRE is negative. This cooling occurs when the solar zenith angle is large and the clouds are of low to medium optical thickness such as late 9 March and early on 10 March (there are other examples mostly associated with cirrus). While the uncertainty is large and the absolute values are small, this effect arises because the albedo increase due to clouds results in less gaseous absorption by water vapor in the lower troposphere.

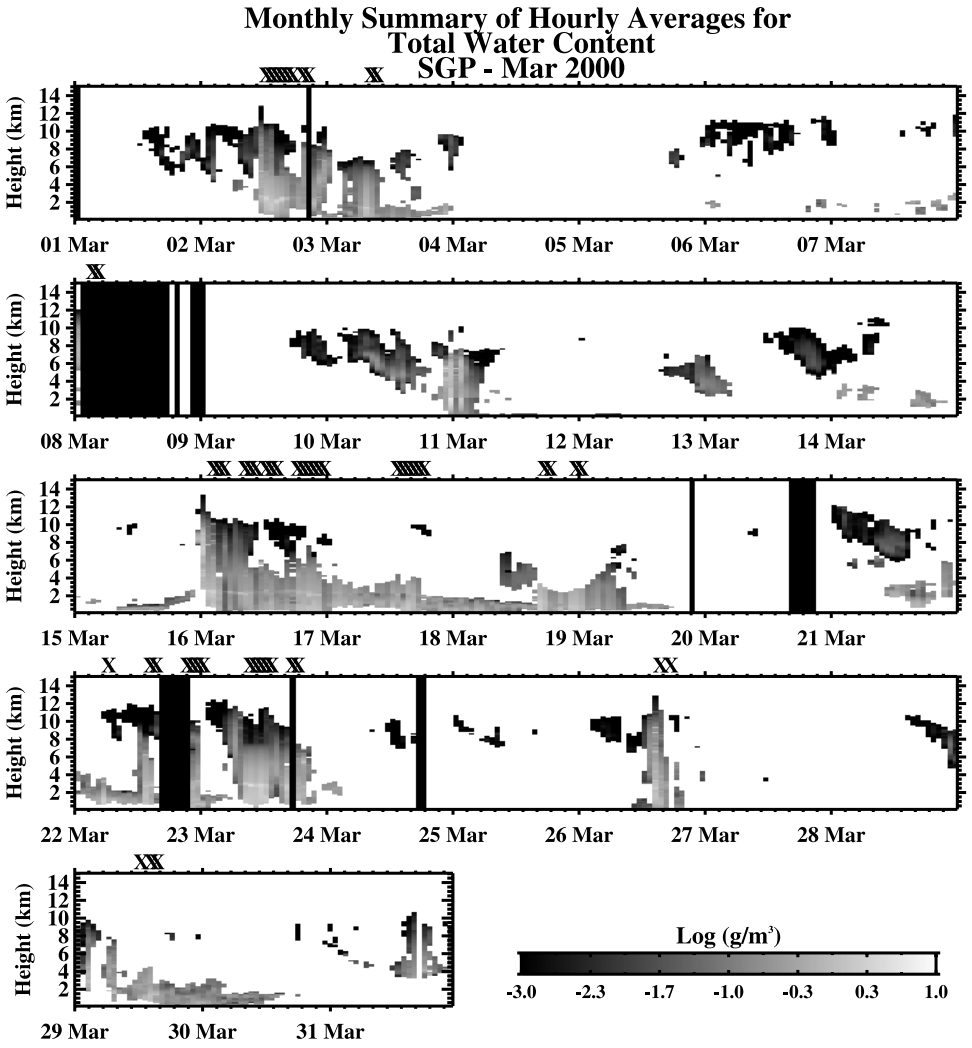

Figure 3. Hourly averages of total condensed water content for March 2000 at the SGP ARM central facility diagnosed using the CPC technique described in part 1. Each row shows a period of days with full rows corresponding to a week of the month. The daily timestamp along the abscissa is situated at the beginning of the UTC day while the ordinate is in kilometers above mean sea level. Areas where black runs vertically from top to bottom denote missing data.

[26] The net atmospheric CRE (Figure 5c) shows how the solar and IR CRE tend to act in opposition when the clouds are optically thick. This opposition is enhanced when cloud tops are in the lower and middle troposphere. Thin cirrus clouds appear to heat the atmosphere as a whole except when the solar cooling effect at high zenith angles is dominant although the uncertainty is large under these conditions. The sign of the atmospheric CRE under middle and high-level clouds of low to moderate optical thickness (i.e., 12, 13, and 21 March) depends on the magnitudes of the solar heating and IR cooling which in turn depend on the cloud microphysical properties, the location of the cloud in the vertical column and the time of day. These results along with the obvious correlation between cloud occurrence and the large-scale dynamics draws attention to the importance of models to correctly predict these cloud properties as a function of location within the synoptic wave and time of day.

[27] While this preliminary analysis of the CRE during March 2000 is enlightening, we have conjectured that much of the resultant effect on the atmosphere is due to CRF of different signs at different altitudes, and as we have discussed previously, the redistribution of energy by clouds is a critical component of the cloud feedback process. In the next section, we examine the CRF and CRE of clouds as a function of type. In our remaining discussion of the March 2000 period, we consider the CRF during the three periods when the large-scale dynamics were more or less consistent. The first and last 10 days of the March 2000 were somewhat similar in that the meteorology was dominated by migratory disturbances that propagated over the SGP region out of the desert southwest while the middle of the month was characterized by a stagnant pattern over the U.S. mid section that brought overrunning clouds and precipitation to the ARM site. The vertical distributions of clouds that were observed during these periods were distinct (Figure 6).

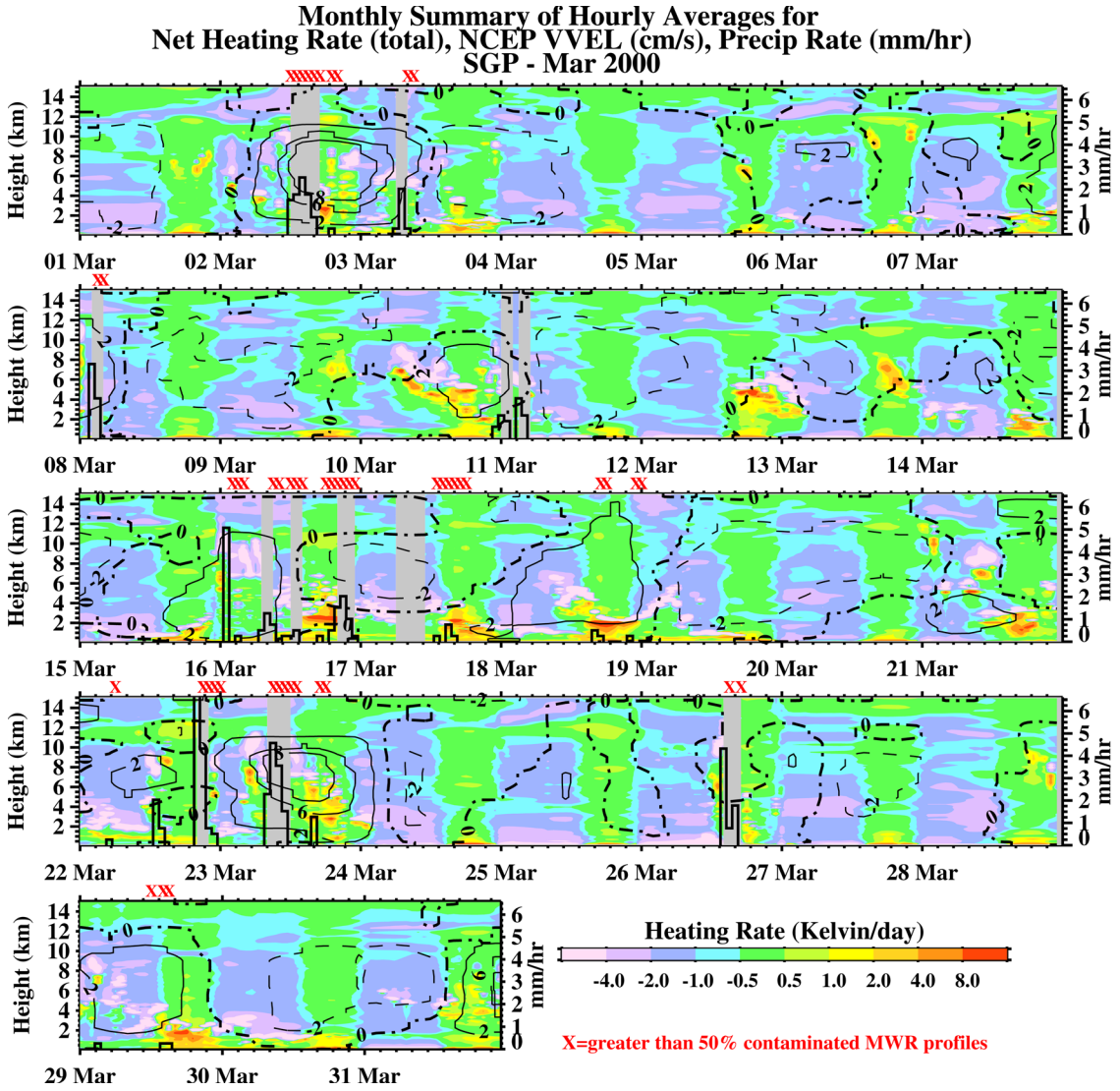

Figure 4. Large-scale vertical motion (contours), precipitation rate (histograms), and net hourly averaged cloud radiative heating rates (color shading) during March 2000 at the Southern Great Plains ARM central facility. Ordinate and abscissa as in Figure 3. Red crosses across the top of the plots denote hours that are likely erroneous because of precipitation.

Clouds during the early third of the month were nearly equally distributed vertically. During the final third of the month more clouds overall were observed and the distribution was more bimodal with a minimum in occurrence in the middle troposphere.

[28] We examine the overall CRF and CRE for these periods and the month as a whole in Figure 7 and Table 2. For this analysis we consider only periods when the sky is generally overcast during 1 hour periods. By considering temporal averages as opposed to a time series of these cloud effects and forcing quantities, the dominance of the IR feedback to the atmosphere during this month is evident. The solar effect at the surface is large and varies generally with the amount and temporal distribution of the cloud cover, but the majority of this cooling (88%) is due to a loss of energy to space through reflection while the remaining fraction is deposited in the atmosphere. The amount of solar heating of the atmosphere is largest under the heavy overcast of the middle 10 days of the month but the uncertainty in the CRF makes this difference difficult to quantify. We can see from Figure 7 that this heating during the middle period of March was concentrated in the lower troposphere below 600 mb with magnitude on the order of 0.5 K day^{-1} although the uncertainty of the magnitudes ranges from 0 to 1 K day^{-1}. The solar heating during the first 10 days was more concentrated in the upper troposphere as opposed to more in the lower troposphere during the final period of March. In the IR, clouds tended to cool the atmosphere during the month with the middle portion of March experiencing more than 30 W m^{-2} of cooling in the atmosphere. Interestingly, we find that the final 10 days of the month were characterized by more IR cooling than the first 10 day period. The atmosphere IR CRE time series in Figure 5c supports this result by inspection. During both

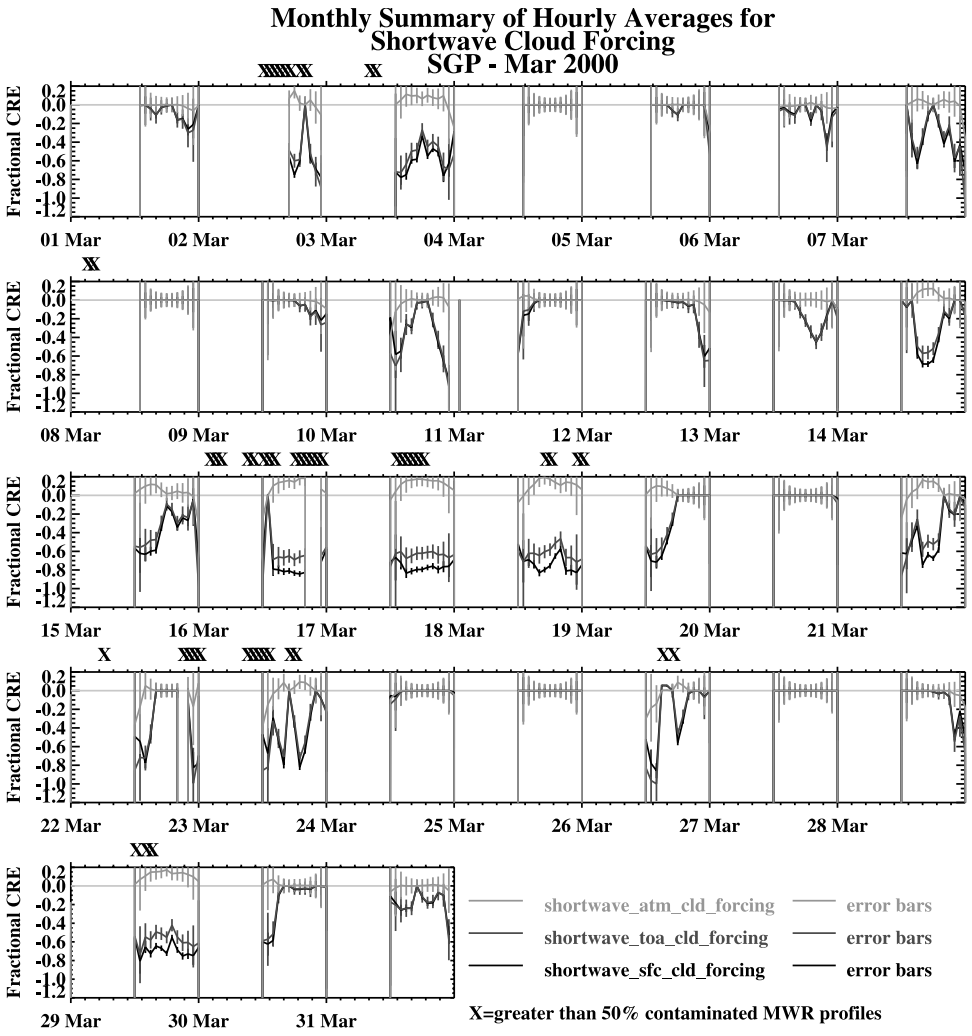

Figure 5a. Cloud radiative effect (CRE) during March 2000 derived from hourly averaged flux calculations for the ARM SGP central facility. The solar CRE is expressed as a fraction of the calculated clear sky downwelling surface solar flux is shown.

10 day periods a single major meteorological event resulted in a persistent period of prolonged negative IR CRE although the heavy cloud cover that passed over the SGP on 29 and 30 March had fairly warm cloud tops relative to the 2–3 March event. This factor resulted in more outgoing longwave energy and cooling of the troposphere. The atmosphere was also somewhat warmer at the end of March compared to the beginning so that cooling due to blackbody radiation was more efficient. These factors are evident in Figure 7, where the averaged IR cooling during the final third of the month is on the order of 3 K day^{-1} and concentrated near 800 mb. While the overcast cloud periods we consider resulted in a net cooling of the atmosphere by approximately 10 W m^{-2} during March, we see that the cooling was not uniform in a vertical sense. The primary cooling took place in the lower troposphere as a result of several persistent low-level cloud events although heating did exist in the upper troposphere when averaged over the month although the precision of this estimated heating is marginal.

4. CRF as a Function of Cloud Type

[29] We have shown with an analysis of March 2000, that the cloud field varied in a time-averaged sense as function of the changing dynamical settings, and the radiative feedbacks to the atmosphere were in turn modulated by the cloud field. However, we also know from intuition and earlier studies [e.g., *Lau and Crane*, 1995; *Stephens*, 2005] that, because clouds form in response to the large-scale dynamics, their occurrence and type are strongly associated with the meteorology. This systematic variability in clouds with the large-scale atmosphere should result in a similar systematically varying diabatic heating feedback to the atmosphere. This coupling has been documented in the oceanic storm tracks [*Weaver and Ramanathan*, 1997] and as a function of large-scale vertical motion [*Tseloudis et al.*, 2000]. The cloud radiative feedbacks to the atmosphere should therefore be considered a strong function of the phasing within the meteorological system where the heating may act to either enhance or dampen the evolving atmospheric circulations through creation or destruction of

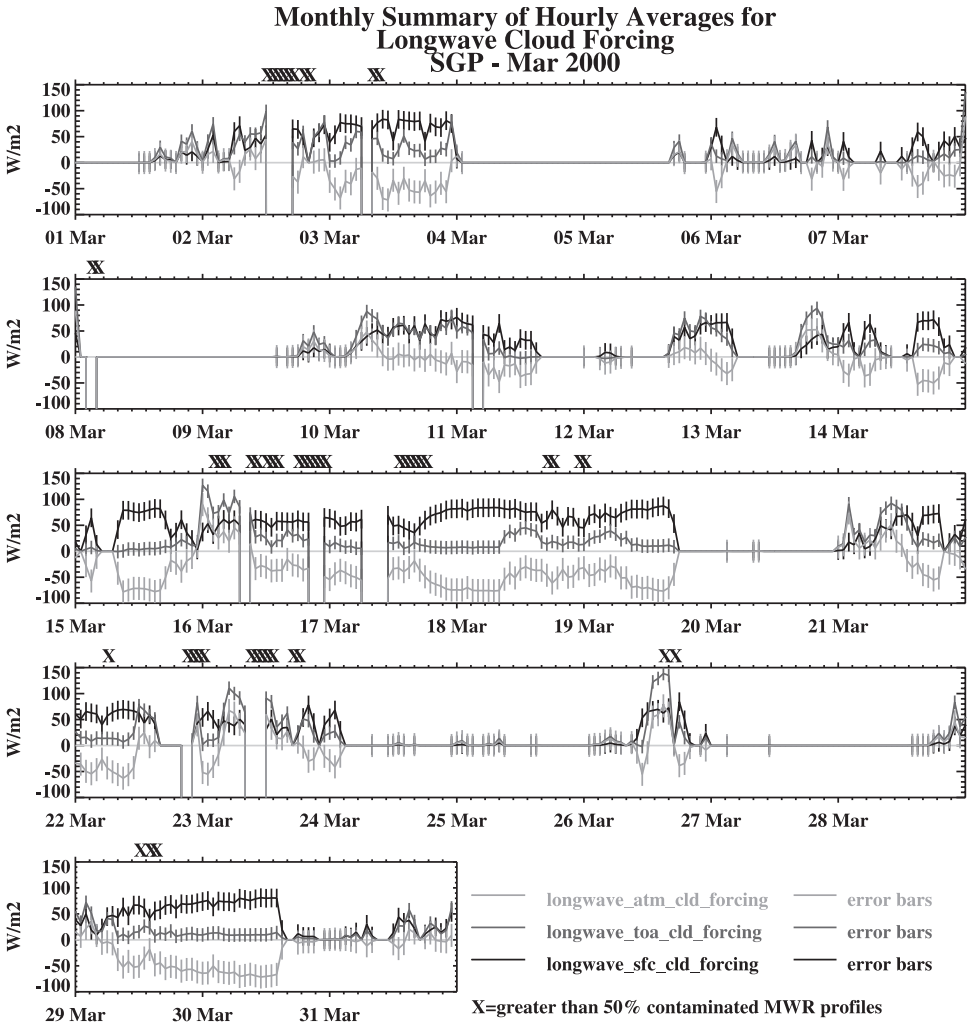

Figure 5b. As in Figure 5a except for the longwave CRE in units of W m^{-2}.

available potential energy [*Webster and Stephens*, 1984; *Stuhlmann and Smith*, 1988]. Using the CPC technique applied to ARM data during the year 2000, we attempt to quantify the CRE and CRF of various cloud types.

[30] To conduct this analysis, it is important to define the clouds types that we are able to evaluate with the ground-based data set. Because the technique we apply to the ground-based data is unable to effectively characterize partially cloudy scenes, we do require the conditions to be generally overcast and of a uniform type. Using the basic cloud type definitions in Table 3, we examine consecutive 1 hour periods and require a single cloud type to be persistent through at least 90% of a given hour before that period is considered for analysis. Once a particular hour is classified as one of the types in Table 3, we collect CRE and CRF statistics from the 5-min data during that hour. Applying this approach to the entire year, we are able to build up an initial description of how a particular cloud type influences the diabatic heating of the atmosphere, surface, and TOA.

[31] We find from Table 3, that a total of 977 overcast hours during the year 2000 were found amounting to approximately 41 full days of data. From Figures 8a–8c, we find that with the exception of an instrument outage in January 2000 (the MWR was down for several days), the monthly frequency of overcast periods reasonably approximates a typical annual cycle of cloud occurrence with a decrease from spring into late summer and then an increase toward the end of the year [*Mace and Benson-Troth*, 2002]. The overcast periods are also distributed more or less evenly through the diurnal cycle. The overcast periods are not evenly distributed among the cloud types with thin high-level clouds and low clouds amounting to nearly 80% of the type-specific hours. Thin high-level clouds were somewhat more likely to be found in the early local evening (0000–0200 UTC) with an annual distribution that is a minimum in late summer (Figure 8b). Low clouds peak in occurrence in March and December with a diurnal occurrence peak in the period around sunrise (1200–1400 UTC). It is difficult to make judgments regarding the temporal distribution of the other cloud types because of the short period under consideration although these preliminary findings seem to make intuitive sense. For instance the deep low clouds that were observed peaked in occurrence during the mid day while the thick high clouds occurred primarily in the local afternoon.

[32] The annually averaged CRE and CRF for the cloud types and all overcast clouds are shown in Table 4 and

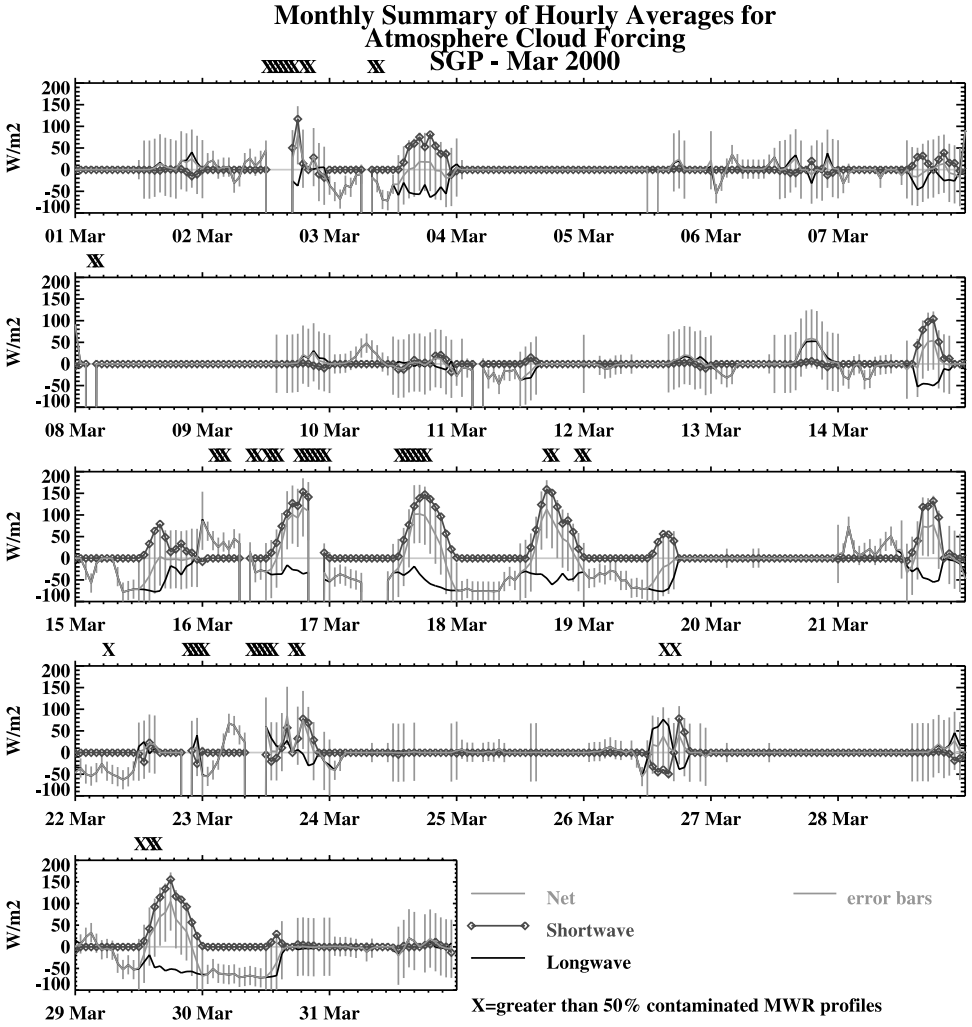

Figure 5c. As in Figure 5a except for the solar, IR and net atmospheric CRE in units of W m^{-2}.

Figures 9a and 9b. For the solar values, we consider the full diurnal cycle. Like the results shown for the March 2000 period, the uncertainty in these results, particularly in the CRF, is substantial. While we can in some circumstances identify heating and cooling without ambiguity, we are, in other circumstances, only able to place bounds on the signs of the terms, and in many instances, even this is not possible. Therefore these results must be considered somewhat preliminary in the sense that analysis of more data to reduce the inherent variability in the fluxes comparisons and improved estimates of the microphysical properties will ultimately result in increased precision.

[33] Low level clouds are unique in that they exert the strongest net cooling influence on the atmosphere. While the TOA value shows that the atmospheric column experiences very strong solar cooling by low-level clouds, approximately 25 W m^{-2} of solar energy is absorbed by low-level clouds in an annual mean sense. In the net, however, the lower troposphere experiences more than 30 W m^{-2} of cooling due to low-level clouds primarily in the northwesterly flow behind cold fronts. While the sample size for low deep clouds is small, we can see a striking and almost certainly realistic difference between the manners in which these two cloud types redistribute radiant energy. Whereas the solar heating by these cloud types, the net TOA CRE, and the surface IR CRE are reasonably similar, the atmosphere IR CRE is significantly different because of the fact that low deep clouds are radiating from cloud tops that are much colder. The low deep clouds are typically of higher visible optical depth and tend to occur preferentially during the day resulting in a larger overall surface solar CRE. The net result on the atmosphere as a whole is indistinguishable from zero for the low deep clouds in contrast to a strong cooling from the low-level overcast clouds.

[34] Overcast middle level clouds, both thin and thick, amount to just 10% of the type-specific overcast hours from the year 2000. These cloud types tended to be observed in the spring and fall seasons. This small occurrence frequency is not a surprise since cloud layers in the middle troposphere are generally less frequent than clouds in the upper and lower troposphere at SGP [*Mace and Benson-Troth*, 2002]. While the thin mid level clouds were distributed evenly throughout the day, the thick mid level clouds that we analyze here peaked in occurrence near local sunrise – although the sample size remains small. Compared to low-level clouds, mid level clouds appear to have much less influence on the solar radiation streams with apparently negligible influence on atmospheric heating. The net effect

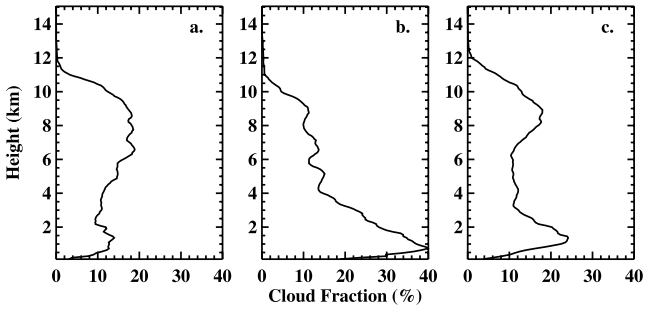

Figure 6. Vertical occurrence fraction of clouds in 90 m range bins as a function of height for (a) 1–9 March, (b) 10–20 March, and (c) 21–31 March 2000.

of these clouds is then determined by their interaction in the IR where cloud top cooling is larger in the thicker clouds offsetting the increased heating near cloud base. The thin mid level clouds on the other hand have weaker heating but apparently small cooling near cloud top resulting in a similar net forcing for these two cloud types on the order of 20 W m^{-2} in the annual mean concentrated primarily in the middle troposphere.

[35] While thick high clouds are a very small component of the data set, it is interesting to contrast their CRE and CRF with the much more common optically thin cirrus. The optically thin cirrus appear similar to the optically thin mid level clouds with primarily IR heating on the order of 20 W m^{-2} concentrated in the upper troposphere and minimal solar heating. The thick high-level clouds have a much stronger influence in the IR with net heating that arises from a pronounced heating-cooling couplet in the upper troposphere. The negative solar CRE for thick high-level clouds arises because of attenuation of solar radiation by the clouds resulting in less gaseous absorption that is realized as a cloud-induced cooling. This effect, since it occurs through the depth of the column (primarily because of water vapor in the lower troposphere), winds up being larger than the direct heating of condensate by absorption.

[36] For the year 2000, we find that the overcast cloud periods exerted a net cooling influence on the surface of approximately 30 W m^{-2} with a small net atmospheric heating that is likely on the order of a few W m^{-2}. Curiously, while we have found that the IR CRE dominated the cloud type specific radiative effect, in the aggregate, the net atmospheric IR CRE is negligible. However, this is somewhat misleading. In Figures 9a and 9b, we find that the solar heating for all overcast clouds, while small and largely within the uncertainty of our calculations, seems to be concentrated in the upper troposphere and in the lower troposphere resulting in a net positive value in the vertical integral. In the IR, while the vertical aggregate is small, we find that this result is due to a cancellation of strong cloud top cooling in the lower troposphere associated with boundary layer clouds and heating that begins in the middle troposphere and extends into the upper troposphere associated with middle and high-level clouds. Our interpretation of this result is that clouds in the atmosphere over this site are tending to redistribute energy vertically beyond what would occur in clear skies. However, this redistribution is a strong function of cloud type and therefore a function of the location within the weather system that is driving cloud formation and maintenance. Furthermore, this effect would be totally missed by passive remote sensors either in space or on the ground that are unable to identify the cloud vertical structure.

5. Summary and Conclusions

[37] Modulation of the large-scale atmospheric circulation by cloud-induced radiative heating has long been recognized as one of the primary feedback mechanisms within the atmosphere. While many seminal studies have used global earth radiation budget measurements from space to document the influence of clouds at the TOA, these studies have been hampered by insufficient information regarding the vertical distribution of clouds within the atmosphere. Therefore the distribution in space and time of cloud-induced heating in the atmosphere is essentially undocumented from data. Because of this lack of observational constraint, the metric for numerical models of the general circulation has been limited to the energy balance at the TOA which, taken alone, is an insufficient constraint. While we have not provided a global measurement of the CRE or CRF in this paper, we have made a first attempt to document the radiative influence of clouds on the atmosphere during a particular month and as a function of cloud type during a particular year at an observational site in Oklahoma.

[38] To accomplish this task, we have exploited the long-term measurements of thermodynamic and cloud properties recorded at the SGP ARM site. These measurements include data from radiosondes and ground-based in situ sensors, and passive measurements of downwelling microwave energy that are converted into integrated liquid and vapor column amounts. To this we add vertically resolved measurements provided by radar, lidar and ceilometer. These data are all combined onto a 90 m vertical and 5 min temporal grid using techniques discussed in detail in part 1 that characterize the physical state of the atmospheric profiles as a function of time over the ARM central facility including cloud location, microphysical properties, radiative properties, and upwelling and downwelling solar and IR radiative fluxes. Validation is provided from various sources including other ground based derivations of column radiative properties [i.e., *Min and Harrison*, 1996] and through comparison with ground-based and TOA flux measurements [*Minnis and Smith*, 1998]. In order to consider the

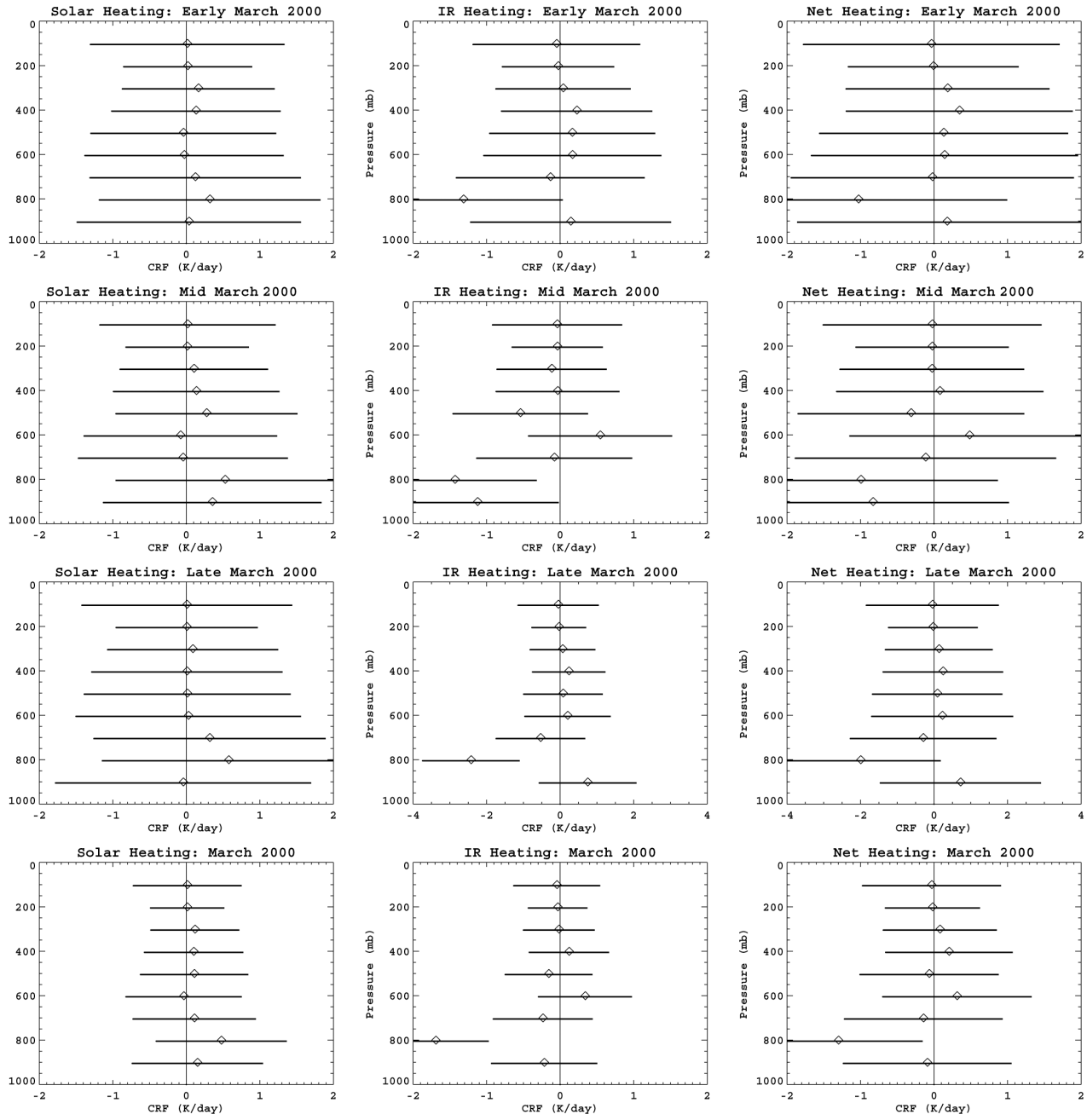

Figure 7. Vertical profiles of the CRF in 100 hPa pressure bins. (left) Solar CRF, (middle) IR CRF, and (right) net CRF. The first, second, and third rows show 1–9 March, 10–20 March, and 21–31 March 2000, respectively. The fourth row shows the entire month of March 2000. The error bars represent the uncertainty calculated using the error propagation methodology described in section 2 and the comparison statistics reported in part 1.

CRE and CRF quantitatively, we used the validation statistics reported in part 1, to estimate the uncertainty in the CRE and CRF using standard error propagation techniques. We find that our skill at estimating common CRE and CRF values is marginal (Table 1) given the precision that we are able to attain with the present set of cloud and radiative property retrieval techniques and the time period considered; this is particularly true for the solar cloud effects. However, in certain circumstances, it is possible to gain understanding about the CRE and CRF with careful analysis and interpretation.

[39] Because the month of March 2000 has emerged as a focus of study by several research groups studying clouds, we focus, as well, on that month. Because cloud types do not form randomly within weather systems, their feedback to the atmosphere is a function of location in space and time. Our goal in emphasizing the March 2000 period is therefore to attempt to simultaneously describe the evolution of the synoptic-scale meteorology, the cloud systems,

Table 2. Cloud Radiative Effect for the Month of March 2000[a]

	Solar	IR	Net
	Surface		
Early March	−95 (5)	+39 (3)	−56 (6)
Mid March	−108 (5)	+58 (3)	−50 (7)
Late March	−56 (5)	+43 (3)	−12 (6)
All March	−88 (3)	+47 (2)	−40 (4)
	Atmosphere		
Early March	+8 (11)	−10 (4)	−3 (12)
Mid March	+13 (13)	−32 (4)	−19 (11)
Late March	+10 (12)	−17 (4)	−7 (13)
All March	+11 (7)	−21 (2)	−10 (8)
	Top of Atmosphere		
Early March	−87 (10)	+28 (3)	−59 (11)
Mid March	−95 (10)	+25 (2)	−69 (11)
Late March	−46 (10)	+26 (3)	−20 (12)
All March	−77 (6)	+26 (2)	−51 (7)

[a]Units are W m^{-2} and the periods covered are from 1–9 March (early March), 10–19 March (mid March), and 20–31 March (late March) and the entire month. Values are means of the period with uncertainty in parentheses.

and the coupled radiative feedback of clouds. We show that the clouds did respond to the dynamical forcing (Figure 6) and that the CRE evolved as a function of cloud type (Figure 7). While cirrus and low clouds resulted in heating and cooling of the upper and lower troposphere, respectively, the effects of clouds in the middle troposphere depended on their vertical location, time of occurrence, and optical thickness. Overall the cloud feedbacks were markedly different for the different dynamical regimes. For instance, clouds during the first third of the month demonstrated a vertical distribution that, while weighted toward upper tropospheric clouds, was somewhat more evenly distributed than either the middle or latter 10 day period of the month. While both the beginning and end of March 2000 were characterized by closed circulations at 500 mb over the southwestern United States, the meteorology and clouds over the SGP region during the latter portion of March 2000 was influenced more by flow out of the subtropics rather than by migratory disturbances propagating onshore along an active polar jet as in the earlier part of March. We speculate that this shift in the storm trajectories from a source region along the polar jet to one more associated with the subtropics was casually related to the differences in the cloud occurrences and resulting radiative effects.

[40] While overall clouds cooled the TOA (51 W m^{-2}), surface (40 W m^{-2}), and atmosphere (10 W m^{-2}) during March 2000, the cloud feedbacks within the atmosphere responded to the vertical distribution of clouds (Table 2 and Figure 7). The March 2000 analysis showed that low-level clouds over SGP resulted in net cooling while upper tropospheric clouds resulted in net heating of the atmosphere. To better quantify this effect and examine a more statistically significant representation of CRE and CRF, we examined the full year 2000 data set, segregated by cloud type (Table 3). A total of 977 hours of overcast data were examined with cloud layers in the upper and lower troposphere dominating the statistics of the overcast periods that we examined. The annual results, while different in the details, were qualitatively similar to the results from the month of March. With net cooling at the TOA (25 W m^{-2}) and surface (32 W m^{-2}) dominated by solar effects, the net effect of clouds on the atmosphere is small and difficult to determine quantitatively although weak cooling of 6 W m^{-2} is estimated. This net atmospheric effect, however, masks a significant cloud type–dependent atmospheric feedback that is dominated by the net cooling influence of low-level clouds (37 W m^{-2}) and the overall heating influence of upper tropospheric clouds (21 W m^{-2}). The other clouds types, while not extremely significant in an annual mean because of their infrequent occurrence relative to overcast thin high clouds and low-level clouds, showed interesting effects that depended largely on the cloud microphysical properties and time of day of their occurrence. Thick upper level clouds, for instance had a strong net heating influence

Table 3. Cloud Type Definition and Occurrence Frequency[a]

Type	Definition	Hours
Low clouds	tops < 3 km, $\tau > 0$	218 (30%)
Deep low	bases < 3 km, tops > 6.5 km, $\tau > 10$	18 (3%)
Thin mid	bases > 3 km, tops < 6.5 km, $\tau < 10$	42 (6%)
Thick mid	3 km < base < 6.5 km, top > 3 km, $\tau > 10$	27 (4%)
Thin high	base > 6.5 km, $\tau < 5$	374 (51%)
Thick high	base > 6.5 km, $\tau > 10$	15 (2%)
High – low	low clouds with high clouds, all τ	34 (5%)
All overcast	no specification as to type	977

[a]The symbol τ refers to visible optical depth. Of the type-specific events, there are a total of 728 hours. The "all overcast" classification refers to all overcast periods that include the specific types and also periods that are of mixed type or not classifiable with the other definitions.

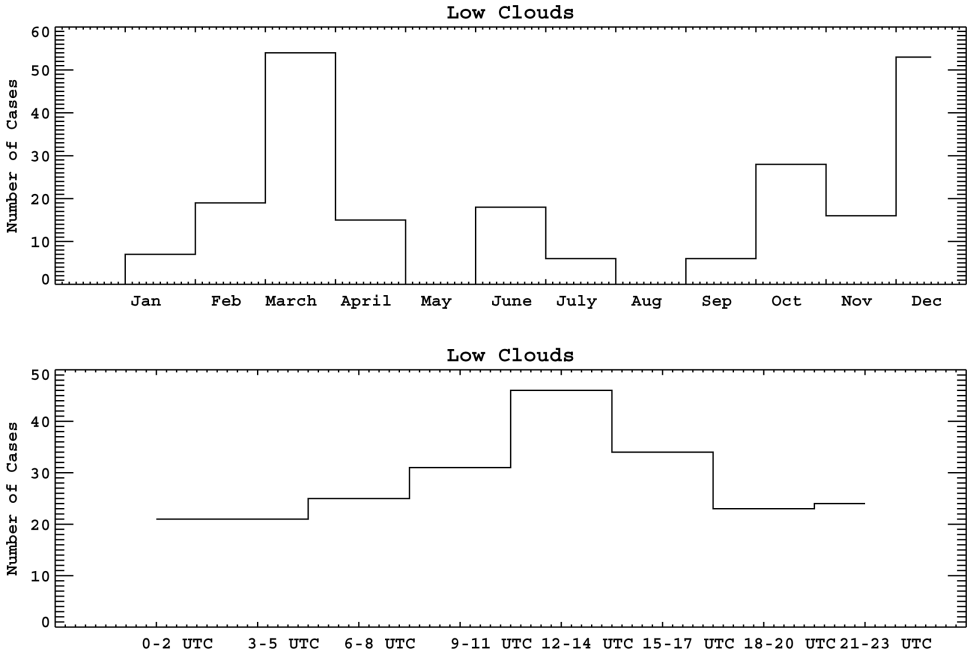

Figure 8a. Frequency distributions of clouds as a function of month and a function of time of day of overcast low clouds.

on the atmosphere that was a balance between a cloud base heating cloud top cooling couplet in the upper troposphere. Thick mid level clouds showed similar characteristics with much less net heating because of relatively warmer cloud tops, while thin mid level clouds responded in a radiatively similar manner to thin cirrus, at least to the degree of uncertainty that we could obtain with this study.

[41] We find by analyzing the CRF of various cloud types over a 1-year period that consideration only of the net radiative effect (CRE) of clouds at the interfaces masks considerable and systematic forcing variability that is a strong function of cloud type, location, and timing within the atmospheric vertical profile. The vertical redistribution of radiant energy by clouds is a strong function of the phasing of the cloud fields within the synoptic-scale system, and since global climate models must accurately predict these feedbacks to the circulation, the correct prediction of the occurrence as a function of location within the synoptic wave is of first-order importance. Correct prediction of the gross microphysical properties seems to be of secondary

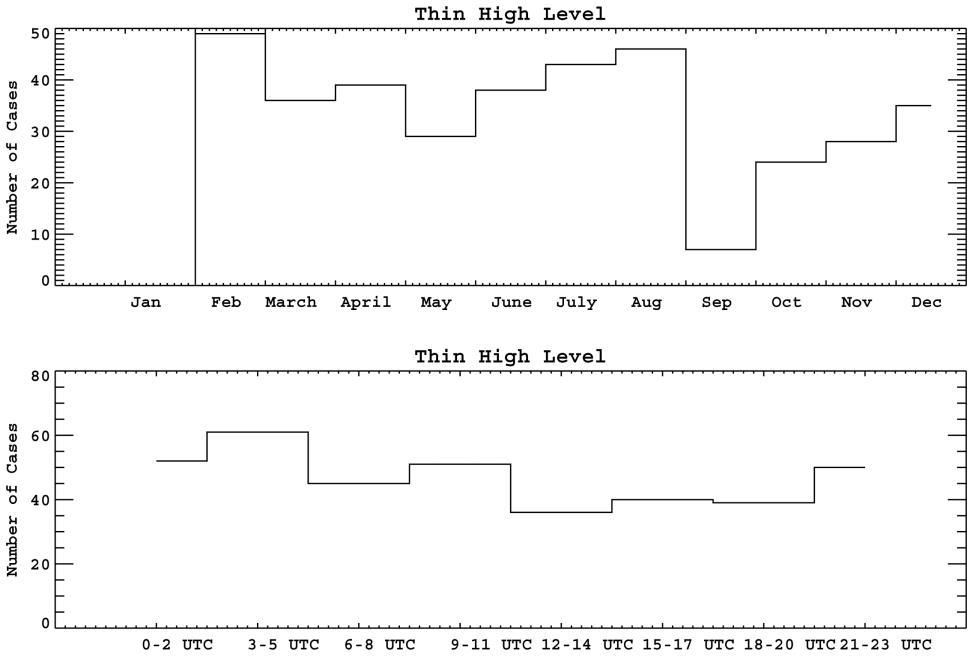

Figure 8b. As in Figure 8a except for overcast thin high clouds.

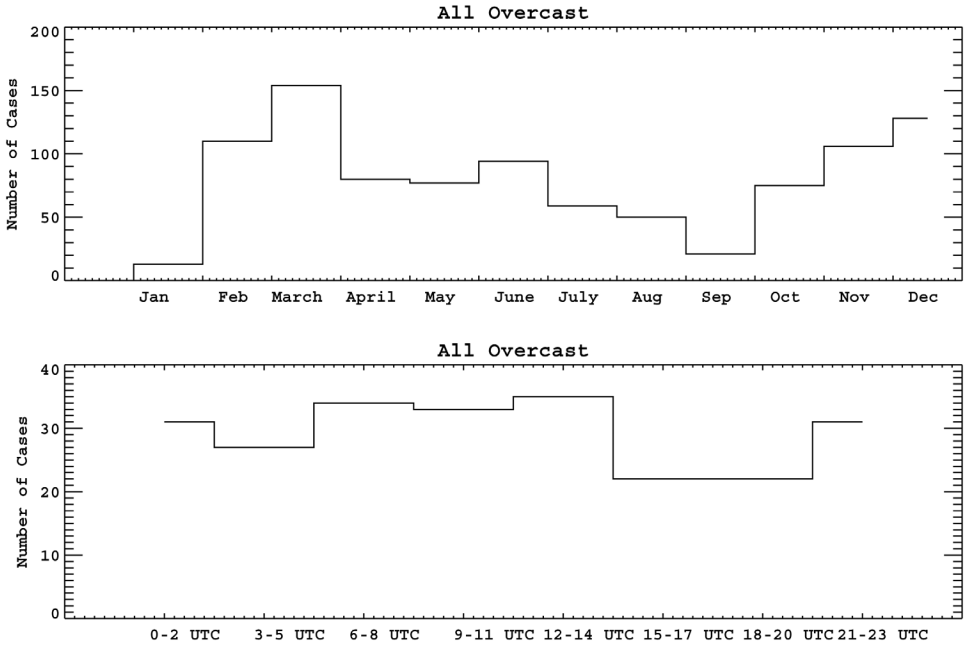

Figure 8c. As in Figure 8a except for all overcast periods.

Table 4. Cloud Radiative Effect at the ARM SGP During the Year 2000 as a Function of Cloud Type[a]

	Solar	IR	Net
	Low Level		
TOA	−130 (7)	+10 (3)	−120 (8)
ATM	+25 (8)	−63 (3)	−37 (9)
SFC	−156 (3)	+73 (2)	−83 (4)
	Low Deep		
TOA	−179 (20)	+60 (4)	−118 (22)
ATM	+17 (21)	−9 (8)	+9 (23)
SFC	−196 (9)	+68 (6)	−127 (11)
	Thin Mid Level		
TOA	−47 (12)	+46 (3)	−1 (14)
ATM	0 (14)	+17 (5)	+17 (16)
SFC	−47 (6)	+29 (4)	−17 (8)
	Thick Mid Level		
TOA	−67 (16)	+71 (4)	+4 (18)
ATM	−1 (17)	+24 (6)	+23 (18)
SFC	−66 (7)	+47 (5)	−18 (9)
	Thin High Level		
TOA	−13 (2)	+29 (1)	+16 (2)
ATM	−1 (5)	+23 (2)	+21 (6)
SFC	−12 (2)	+6 (1)	−6 (2)
	Thick High Level		
TOA	−138 (22)	+107 (6)	−30 (23)
ATM	−17 (25)	+87 (9)	+69 (27)
SFC	−119 (10)	+21 (7)	−99 (12)
	Low-High		
TOA	−83 (14)	+49 (3)	−35 (15)
ATM	+10 (16)	−16 (6)	−6 (17)
SFC	−93 (6)	+65 (4)	−29 (8)
	All Overcast		
TOA	−56 (3)	+31 (1)	−25 (3)
ATM	+6 (3)	+1 (1)	+6 (3)
SFC	−62 (2)	+30 (1)	−32 (2)

[a]All units are W m^{-2} and the uncertainty is shown in parentheses. Quantities shown are for overcast skies of the indicated type.

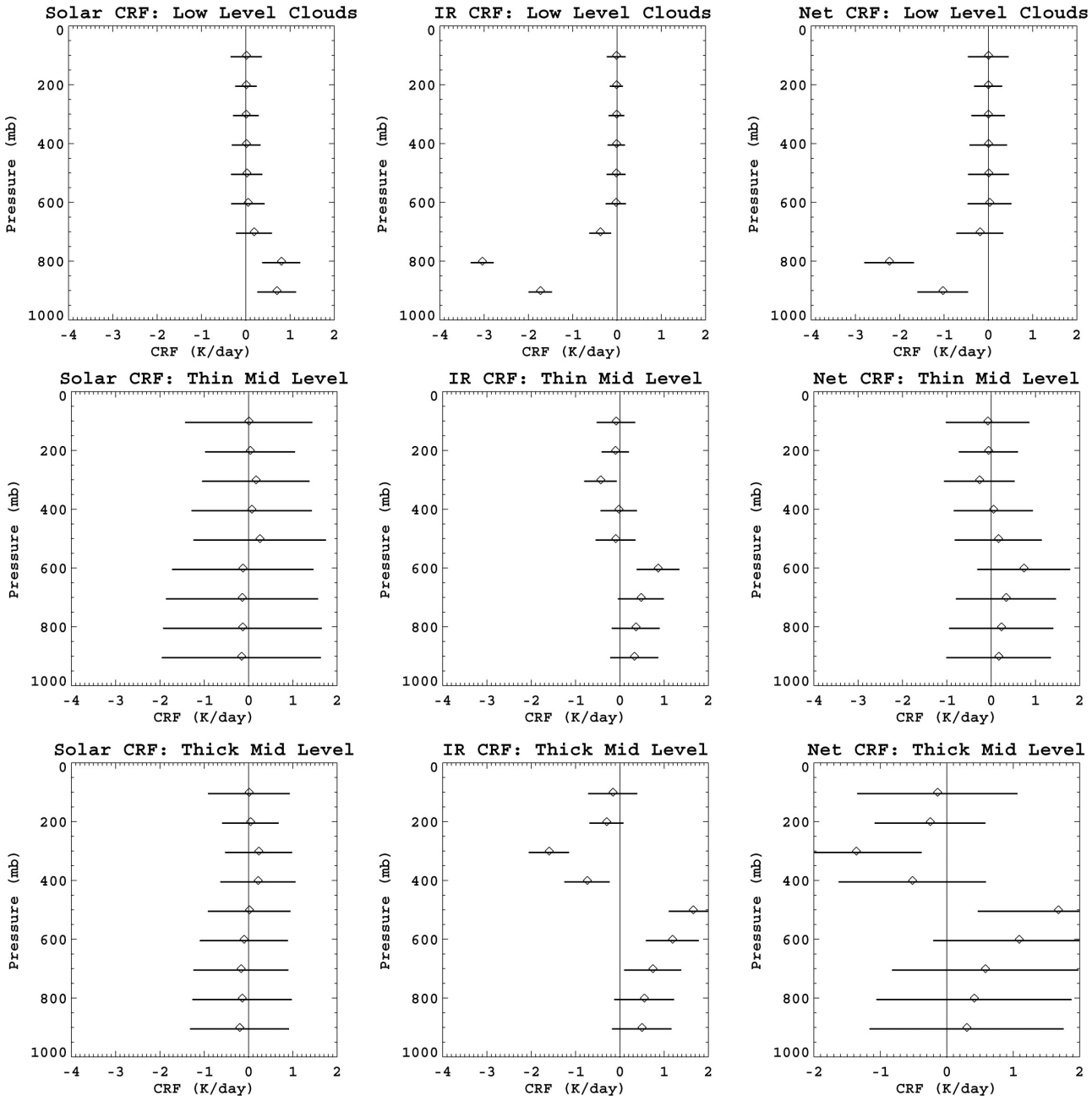

Figure 9a. Profiles of the CRF (K/day) for the (left) solar, (middle) IR, and (right) net flux for various cloud types as defined in Table 3 listed in the title of each plot. The error bars represent the uncertainty calculated using the error propagation methodology described in section 2 and the comparison statistics reported in part 1.

importance overall since the majority of the feedbacks (at least over this ground site during this period of time) are primarily determined by thin cirrus and optically thick boundary layer clouds. Clearly, predicting the location and timing of these clouds is very important to accurately modeling cloud feedbacks in the atmosphere.

[42] This work (parts 1 and 2) represents a first attempt at using ground-based measurements to characterize the radiative effect of clouds on monthly and annual timescales. Significant work remains to be accomplished. Because we have carefully limited our analysis to overcast periods, our results do not include the effects of partly cloudy skies. In the absence of scanning millimeter radar, it will be necessary to merge the vertically pointing measurements with additional data sources such as sky imagers that provide information on the spatial distribution of clouds. From a technology standpoint, improved representations of cloud microphysics are necessary that can quantitatively demonstrate an improvement in our ability to characterize the cloud forcing of a particular cloud type. This need is especially relevant to mixed phase clouds where the liquid water has the potential of dominating the cloud radiative

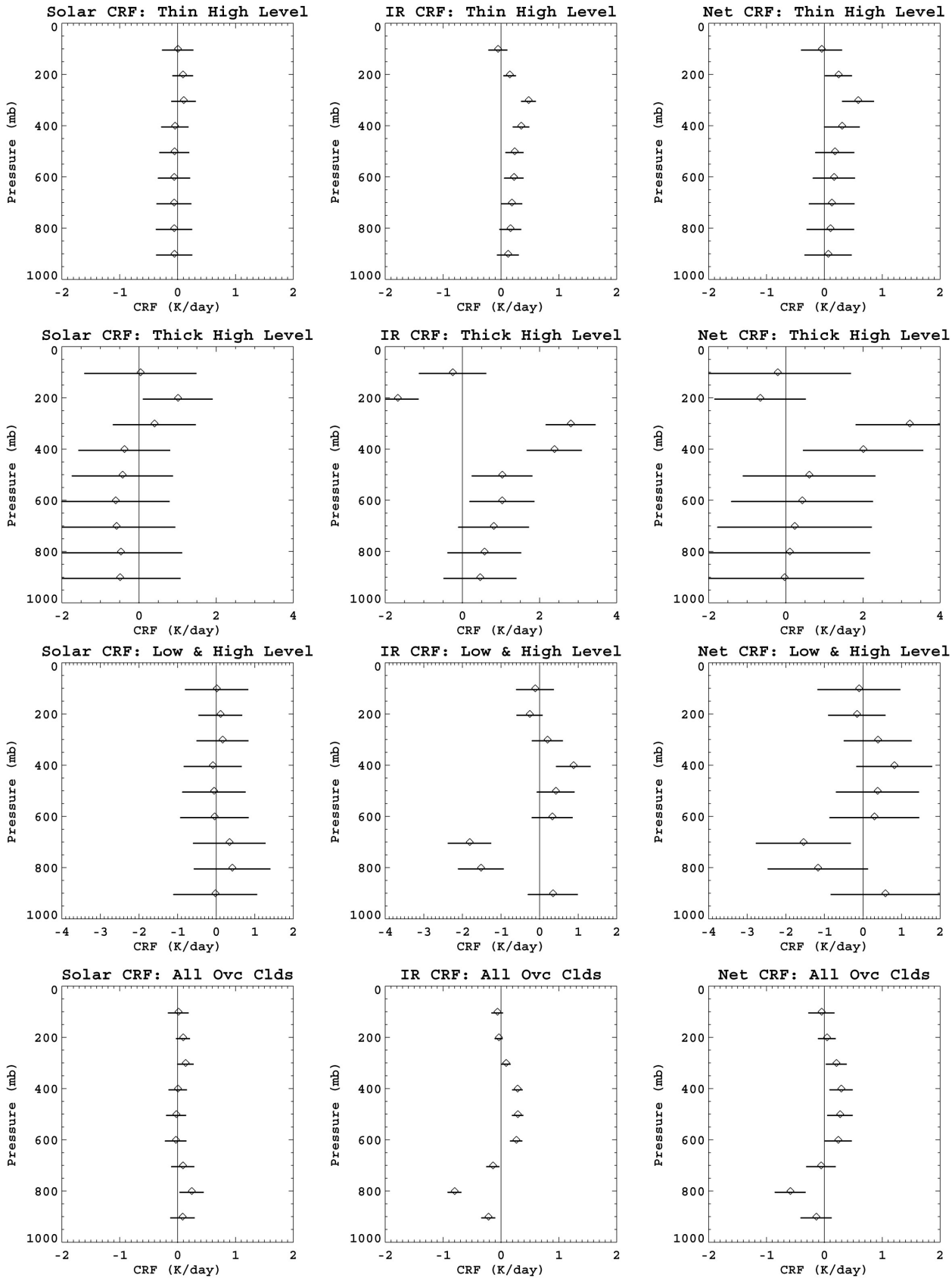

Figure 9b. As in Figure 9a except for additional cloud types as shown in the legend of the plots.

properties. While mixed phase clouds tend to be optically thick, identifying the vertical location in the column where the clouds become optically thick from the top is important for accurately estimating the radiative feedbacks of these clouds. Algorithms that estimate the liquid water content and particle size profiles in the presence of large ice crystals that dominate the Doppler radar signature is a significant challenge. Unlike boundary layer clouds where we have an integral constraint on the column liquid, no such constraint exists for cirrus. Therefore improvement in cirrus retrieval algorithms are also needed given the dominance of cirrus in the cloud occurrence distributions.

[43] Since clouds are closely coupled to the large-scale meteorology, the ARM data present many opportunities for quantifying this association. By extending our analysis to multiple years, it will be possible to develop composites of cloud properties that are segregated by the dynamical regimes in which they exist. This analysis approach will provide a powerful validation tool for models and can also provide a roadmap for focused studies into cloud systems that are poorly understood. Certainly, extension of these results to other climate regimes is also necessary and possible with ARM data. However, we look forward to eventual global distributions of cloud properties derived from the active and passive remote sensors on the A-Train satellites [*Stephens et al.*, 2002].

[44] **Acknowledgments.** This research work was first discussed when two of the authors (G.M. and S.K.) were graduate students of T. Ackerman at Penn State, and we gratefully acknowledge T. Ackerman's influence and guidance. We also thank E. E. Clothiaux at Penn State for providing a part of the radiative transfer code. Funding for this work was provided by the Environmental Science Division of the U.S. Department of Energy (grant DE-FG0398ER657). Data were obtained from the Atmospheric Radiation Measurement Program sponsored by the U.S. Department of Energy, Office of Science, Office of Biological and Environmental Research, Environmental Science Division. S.K. is supported by a NASA grant of the Clouds and the Earth's Radiant Energy System (CERES) project grant (NNL04AA26G).

References

Barkstrom, B. R., E. F. Harrison, and R. B. Lee III (1990), Earth Radiation Budget Experiment: Preliminary seasonal results, *Eos Trans. AGU*, *71*(9), 297, 304.

Bergman, J. W., and H. H. Hendon (1998), Calculating monthly radiative fluxes and heating rates from monthly cloud observations, *J. Atmos. Sci.*, *55*, 2471–3491.

Bergman, J. W., and H. H. Hendon (2000), Cloud radiative forcing of the low-latitude tropospheric circulation. Linear Calculations, *J. Atmos. Sci.*, *57*, 2225–2245.

Bevington, P. R., and D. K. Robinson (1992), *Data Reduction and Error Analysis for the Physical Sciences*, McGraw-Hill, New York.

Chen, T., W. B. Rossow, and Y. Zhang (2000), Radiative effects of cloud-type variations, *J. Clim.*, *13*, 264–286.

Dong, X., and G. G. Mace (2003), Profiles of low-level stratus cloud microphysics deduced from ground-based measurements, *J. Atmos. Oceanic Technol.*, *20*, 45–53.

Fu, Q. (1996), An accurate parameterization of the solar radiative properties of cirrus clouds for climate models, *J. Clim.*, *9*, 2058–2082.

Fu, Q., P. Yang, and W. B. Sun (1998), An accurate parameterization of the infrared radiative properties of cirrus clouds for climate models, *J. Clim.*, *9*, 2223–2237.

Kato, S., T. P. Ackerman, J. H. Mather, and E. E. Clothiaux (1999), The k-distribution method and correlated-k approximation for a shortwave radiative transfer model, *J. Quant. Spectrosc. Radiat. Transfer*, *62*, 109–121.

Kato, S., G. L. Smith, and H. W. Barker (2001), Gamma-weighted discrete ordinate two-stream approximation for computation of domain-averaged solar irradiance, *J. Amos. Sci.*, *58*, 3797–3803.

Kiehl, J. T., J. J. Hack, and B. P. Briegleb (1994), The simulated Earth radiation budget of the National Center for Atmospheric Research Community Climate Model CCM2 and comparisons with the Earth Radiation Budget Experiment (ERBE), *J. Geophys. Res.*, *99*(D10), 20,815–20,827.

Kiehl, J. T., J. J. Hack, G. B. Bonan, B. A. Boville, D. L. Williamson, and P. J. Rasch (1998), The National Center for Atmospheric Research Community Climate Model: CCM3, *J. Clim.*, *11*, 1131–1149.

Lau, N.-C., and M. W. Crane (1995), A satellite view of the synoptic-scale organization of cloud properties in midlatitude and tropical circulation systems, *Mon. Weather Rev.*, *123*(7), 1984–2006.

Lau, N.-C., and M. W. Crane (1997), Comparing satellite and surface observations of cloud patterns in synoptic-scale circulation systems, *Mon. Weather Rev.*, *125*(12), 3172–3198.

Lau, K.-M., C.-H. Ho, and M.-D. Chou (1996), Water vapor and cloud feedback over the tropical oceans: Can we use ENSO as a surrogate for climate change?, *Geophys. Res. Lett.*, *23*(21), 2971–2974.

Liu, C., and A. J. Illingworth (2000), Toward more accurate retrievals of ice water content from radar measurements of clouds, *J. Appl. Meteorol.*, *39*, 1130–1146.

Long, C. N., and T. P. Ackerman (2000), Identification of clear skies from broadband pyranometer measurements and calculation of downwelling shortwave cloud effects, *J. Geophys. Res.*, *105*(D12), 15,609–15,626.

Mace, G. G., and S. Benson-Troth (2002), Cloud overlap characteristics derived from long-term cloud radar data, *J. Clim.*, *15*, 2505–2515.

Mace, G. G., K. Sassen, S. Kinne, and T. P. Ackerman (1998), An examination of cirrus cloud characteristics using data from millimeter radar and lidar: The 24 April SUCCESS case study, *Geophys. Res. Lett.*, *25*, 1133–1136.

Mace, G. G., A. J. Heymsfield, and M. R. Poellot (2002), On retrieving the microphysical properties of cirrus using millimeter wave Doppler moments data, *J. Geophys. Res.*, *107*(D24), 4815, doi:10.1029/2001JD001308.

Mace, G. G., et al. (2006), Cloud radiative forcing at the Atmospheric Radiation Measurement Program climate research facility: 1. Technique, validation, and comparison to satellite-derived diagnostic quantities, *J. Geophys. Res.*, *111*, D11S90, doi:10.1029/2005JD005921.

Miloshevich, L. M., H. Voemel, A. Paukkunen, A. J. Heymsfield, and S. J. Oltmans (2001), Characterization and correction of relative humidity measurements from Vaisala RS80-A radiosondes at cold temperatures, *J. Atmos. Oceanic Technol.*, *18*(2), 135–156.

Min, Q.-L., and L. C. Harrison (1996), Cloud properties derived from surface MFRSR measurements and comparison with GOES results at the ARM SGP site, *Geophys. Res. Lett.*, *23*, 1641–1644.

Minnis, P., and W. L. Smith Jr. (1998), Cloud and radiative field derived from GOES-8 during SUCCESS and the ARM-UAV Spring 1996 Flight Series, *Geophys. Res. Lett.*, *25*, 1113–1116.

Minnis, P., K.-N. Liou, and Y. Takano (1993), Inference of cirrus cloud properties using satellite-observed visible and infrared radiances. Part I: Parameterization of radiance fields, *J. Atmos. Sci.*, *50*(9), 1279–1304.

Mlawer, E. J., S. J. Taubman, P. D. Brown, M. J. Iacono, and S. A. Clough (1997), Radiative transfer for inhomogeneous atmospheres: RRTM, a validated correlated-k model for the longwave, *J. Geophys. Res.*, *102*, 16,663–16,682.

Norris, J. R., and C. P. Weaver (2001), Improved techniques for evaluating GCM cloudiness applied to the NCAR CCM3, *J. Clim.*, *14*, 2540–2551.

Ramanathan, V., and W. D. Collins (1991), Thermodynamic regulation of the ocean warming by cirrus clouds deduced from observations of the 1987 El Nino, *Nature*, *351*, 27–32.

Rossow, W. B., and R. A. Schiffer (1999), Advances in understanding clouds from ISCCP, *Bull. Am. Meteorol. Soc.*, *80*, 2261–2288.

Rossow, W. B., and T.-C. Zhang (1995), Calculation of surface and top of atmosphere radiative fluxes from physical quantities based on ISCCP data sets: 2. Validation and first results, *J. Geophys. Res.*, *100*, 1167–1197.

Sherwood, S. C., V. Ramanathan, T. P. Barnett, M. K. Tyree, and E. Rocckner (1994), Response of an atmospheric general circulation model to radiative forcing of tropical clouds, *J. Geophys. Res.*, *99*(D10), 20,829–20,845.

Slingo, A. (1989), A GCM parameterization for the shortwave radiative properties of water clouds, *J. Atmos. Sci.*, *46*(10), 1419–1427.

Sohn, B.-J. (1999), Cloud induced infrared radiative heating and its implications for large-scale tropical circulations, *J. Atmos. Sci.*, *56*, 2657–2672.

Stephens, G. L. (2005), Cloud feedbacks in the climate system: A critical review, *J. Atmos. Sci.*, *18*, 237–273.

Stephens, G. L., et al. (2002), The CloudSat mission and the A-Train, *Bull. Am. Meteorol. Soc.*, *83*, 1771–1790.

Stuhlmann, R., and G. L. Smith (1988), A study of cloud-generated radiative heating and its generation of available potential energy. Part I: Theoretical background, *J. Atmos. Sci.*, *45*, 3911–3927.

Toon, O. B., C. P. McKay, T. P. Ackerman, and K. Santhanam (1989), Rapid calculation of radiative heating rates and photodissociation rates in inhomogeneous multiple scattering atmospheres, *J. Geophys. Res.*, *94*(D13), 16,287–16,301.

Tseloudis, G., Y. Zhang, and W. B. Rossow (2000), Cloud and radiation variations associated with northern midlatitude low and high sea level pressure regimes, *J. Clim.*, *13*, 312–327.

Weaver, C. P., and V. Ramanathan (1997), Relationships between large-scale vertical velocity, static stability, and cloud radiative forcing over Northern Hemisphere extratropical oceans, *J. Clim.*, *10*, 2871–2887.

Webster, P. J. (1994), The role of hydrological processes in ocean-atmosphere interactions, *Rev. Geophys.*, *32*(4), 427–476.

Webster, P. J., and G. L. Stephens (1981), Clouds and climate: Sensitivity of simple systems, *J. Atmos. Sci.*, *38*(2), 235–247.

Webster, P. J., and G. L. Stephens (1984), Cloud-radiation interaction and the climate problem, in *The Global Climate*, edited by J. Houghton, pp. 63–78, Cambridge Univ. Press, New York.

Weilicki, B. A., et al. (1998), Clouds and the Earth's radiant energy system (CERES): Algorithm overview, *IEEE Trans. Geosci. Remote Sens.*, *36*(4), 1127–1141.

Zhang, M. H., et al. (2005), Comparing clouds and their seasonal variations in 10 atmospheric general circulation models with satellite measurements, *J. Geophys. Res.*, *110*, D15S02, doi:10.1029/2004JD005021.

S. Benson and G. G. Mace, Department of Meteorology, University of Utah, Salt Lake City, UT 84112-0110, USA. (mace@met.utah.edu)

S. Kato, Center for Atmospheric Sciences, Hampton University, Hampton, VA 23668, USA.